



Stay in Place Formwork, Encased Reinforced Concrete Column: A Review

Zainab H. Abbas^{a*}, Maan S. Hassan^a, Iqbal N. Gorgis^b

^aCivil Engineering Dept., University of Technology-Iraq, Alsina'a street, 10066 Baghdad, Iraq.

^bCivil Engineering Dept., University of Catholic, Erbil, Iraq.

*Corresponding author Email: bce.20.04@grad.uotechnology.edu.iq

HIGHLIGHTS

- SIP formwork offers a cost-effective alternative to classic formwork systems, reducing construction expenses
- The review covers various types of SIP formworks for columns, including PVC, CFRP, steel tubes, and composite material
- The study explores the mechanical features and confinement efficiency of some SIP formwork types for RC columns
- The provides valuable insights for future research in this field

ARTICLE INFO

Handling editor: Qusay F. Alsally

Keywords:

Stay-in-place formwork; column; CFRP; confinement ratio; deformation; compressive strength.

ABSTRACT

Formwork systems are required for almost all cast-in-place concrete construction. However, some forms cost too much, often exceeding 30% of the entire cost of the concrete construction. Thus, the stay-in-place (SIP) formwork, a premanufactured permanent constructional member that holds fresh concrete to the intended sizes and stays in the site to afford loads over the construction lifecycle, could be an auspicious alternative to the classic formwork procedure. Several types of stay-in-place (SIP) formworks for columns have been reviewed, like PVC tubes, CFRP, steel tubes, and the composite of two or more types of stay-in-place (SIP) formwork used together. Moreover, some types of concrete and mortar used as stay-in-place (SIP) formwork have been reviewed. The mechanical, restraint, and deformability characteristics of several types of stay-in-place (SIP) formwork system for concrete columns is discussed. Further, the effect of change in the thickness of several kinds of stay-in-place formworks is highlighted. The impact of the change in the strength level of the core of concrete-filled stay-in-place formworks on the confinement efficiency of stay-in-place formwork is also investigated. Finally, the recommendations for futurity researchers in this area are introduced.

1. Introduction

Concrete is an essential part of the construction materials as it has been used by the Romans. Formwork plays an important role in supporting geometry comprehension and strength development of concrete elements. The selection of a suitable framework is important in any project because it bears about 25% to 30% of the total construction cost. Various formwork systems have been used in different projects. In the design and selection of the formwork system, the requirements, such as safety, cost, structural geometry, construction time, and surface quality, need to be taken into account [1,2].

SIP formwork is a remaining formwork method that structurally collaborates with the concrete and works as a self-bearing formwork during building processes. SIP formworks could increase the bearing capacity and some mechanical properties of concrete. Moreover, some types of SIP formwork could extend the service life of structures exposed to severe environments like marine structures [3]. Various advantages and disadvantages of some types of SIP formwork systems will be explained later in this paper. Moreover, the large-size square concrete-steel hybrid multi-tube concrete column (MTCCs) with PEN (polyethene naphthalate) FRP (Fiber-reinforced polymer (FRP) appeared ascendant ductility because of the influential reservation supplied by PEN FRP coat and steel tubes [4]. Moreover, in offshore implementations, reinforced thermoplastic pipes (RTPs) are considered a good substitute for metallic tubes like steel. The performance of RTPs was considerably enhanced by the development of buckling and collapse strength of RTPs against bending tension loads [5].

Plastic polymer is frequently lighter, cheaper, and has lower thermal conductivity with almost 0.40–0.55% as compared with steel [5-7]. Some polymers like PVC have good fire resistance and prohibit spreading fire.

The preceding literature has suggested and inspected the total construction of concrete structure. Despite the very high cost of the formwork system, including the cost of the materials of formwork, producing labour, and the re-use and huddling of formwork material, almost all of the cast-in-place concrete construction requires a formwork system. To overcome these disadvantages of formwork systems, the SIP formwork is a promising alternative to the classical formwork style, a premanufactured permanent structural member that holds fresh concrete to the intended sizes and stays in the site to afford loads over the construction lifecycle. The present review aims to summarize the existing state of knowledge on the new composite

configuration, concrete padded some types of SIP formwork columns, and promote a substantial understanding of the factors that impact its attitude. The article's outcome highlights the issues and creates a new direction for future authors.

1.1 SIP Formwork Types

1.1.1 Steel tube

Steel tube is a familiar sample of a remaining column formwork [8]. It enhances the columns' strength and ductility by restraining core concrete [9-19]. However, the side effect of the steel tube remaining formwork is the complexity of the linkage with the beam. Also, it had poor strength against fire and corrosion [8,20,21].

1.1.2 Fiber-reinforced polymer (FRP) tubes

FRP tubes have a high strength-to-weight ratio [22,23]. Also, FRP permanent tubes have superior corrosion resistance [24-33]. They provided superior compressive power and ultimate strain of concrete through the confinement of fibers in the hoop direction [34,35]. However, the side effects of FRP tube remaining formwork are poor fire resistance and the release of toxic gases on fire that should be considered [36].

1.1.3 Un-plasticized polyvinyl chloride (uPVC) tubes remaining formwork

UPVC tubes protected reinforced concrete columns from chemical attacks, increased the corrosion resistance of steel in a harsh environment, and prevented the peeling of concrete cover. Also, the columns' strength, ductility, and energy absorption improved by lateral confinement of uPVC to the concrete column [37-43].

1.1.4 Prefabricated textile reinforced concrete (TRC)

Prefabricated textile reinforced concrete (TRC) [44-46], engineered cementitious composites (ECC) [47] and lightweight concrete remaining formwork [48] are novel alternatives to the classical wood/steel formwork organizes.

1.1.5 The remaining formwork of Ultra-high-performance concrete (UHPC)

UHPC-concrete formwork is an attractive formwork that remarkably enhanced load-carrying capability and elastic modulus Tian et al. [49]. The wonderful mechanical properties of UHPC, such as superior elevated compressive strength, high flexural strength, high ductility, toughness, and high durability [50], lead to the possibility of creating a lightweight, durable, and fire-proof SIP formwork.

1.2 Material and Geometric Properties of SIP Formwork

The geometrical parameters: thickness (t) and cross-section dimension; mechanical properties (tensile, compressive features, modulus of elasticity (E), tensile yield strength (fy), ultimate tensile (ft) or compressive strength (fc), and Poisson's ratio (μ)) of the stay-in-place formwork recorded in antecedent studies are offered in Table 1.

Table 1: Features of Stay-in-place formwork

type of SIP formwork	t (mm)	Cross section dimensions (mm)	E (GPa)	fy (MPa)	ft (MPa)	fc (comp. strength) (MPa)	Poisson's ratio (μ)	Ref.
CFRP-PVC tubular (CFCT)	CFRP 1layer 0.17 PVC 4.5	PVC tube (200,600,4.5) external diameter, length, and thickness respectively	36.6 for concrete 2.7×10^5 for CFRP		CFRP= 4.23×10^3	36.6= concrete cube 42.5=PVC tube	PVC =0.36	[51]
Unplasticized polyvinyl chloride (UPVC)		UPVC outer diameters: (55,83and 110) mm. with thicknesses (of 2.5, 3.0 and 2.5) mm, respectively. h/D (slender ratio)=(2,3 & 4)	UPVC=3		UPVC=40	UPVC=59 Concrete cube=(20.7, 27.2 & 30.7)	UPVC=0.38	[52]
PVC	thicknesses (3.7,5.2 and 8.5)	PVC outer diameters 110 & length 220 mm. with thicknesses (3.7, 5.2 and 8.5) mm	PVC=3		PVC=45	(C30=34.9, C45=58 & C60=74.9) PVC pipes= (0.6, 1.0 & 1.6 MPa) for (3.7, 5.2 & 8.5) mm thickness respectively.		[6]

Table 1: Continued

Steel tube		Steel tube: (Group-1 i.e., specimen 1-4 Diameter=165.2mm, thickness=3.7mm). (Group-2, i.e., specimen 5-6 Diameter=230mm, thickness=2.3mm). Whole paradigms were destined to have the same length-to-diameter ratio= 3.				Compressive strength for (Group-1, i.e., 1,2,3,4) = (29.5, 43.5, 58, 81.6) MPa respectively, and for (Group-2, i.e. 5,6) (32 & 64) MPa respectively. For Steel tube yield strength=(366 MPa for group-1 and 360.8 MPa for Group-2)	[53]	
grid-reinforced ultra-high-performance concrete (UHPC)	(20 & 40)	240 mm in diameter and 600 mm in height.	Modulus of elasticity of reinforcement CFRP grid & (SS) grid: 167 & 210 GPa, respectively.	The yield strength of reinforcement steel & stainless steel (SS) grid is 417.2 & 442.6 MPa, respectively.	The maximum strength of reinforcement steel (SS) & CFRP grid: (563.7, 737.4 & 3459.3).	Compressive strength of UHPC-SIP formwork and core concrete: (139.3 & 32.4) MPa, respectively.	[49]	
Composite columns: AFS-Logiwall (LW) and AFS-Rediwall (RW). Reference column: Standard columns (STCs)	thickness: (6 & 3) for Fiber cement board (FCB) & PVC, respectively.	AFS- LW (188x600x1200) STC (188x600x1200) AFS- RW (256x600x1200) STC (256x600x1200)	Modulus of elasticity of core concrete & FCB: (24 & 5) GPa, respectively.	Yield strength of FCB: 4.95 MPa.	Ultimate tensile strength of core concrete & FCB: (2.7 & 5.95) MPa, respectively.	Compressive strength of core concrete & FCB: (20 & 52) MPa, respectively.	0.2 for each core concrete and FCB	[54]
3D printed-precast permanent concrete formwork.	25 mm	Diameter X length: (250x 600) mm for all columns.				Compressive strength of printed & core concrete (40 & 30) MPa, respectively.	[55]	

2. Mechanical Properties of Composite Column (SIP Formwork Confined Concrete)

Some mechanical properties such as confined strength, unconfined strength, the ratio of confinement strength effectiveness, and the ratio of confined to unconfined strain of various types of composite columns from several researchers are explained in Table 2. It was clear that the increase in the formwork thickness for any type of SIP formwork caused an increase in the confinement strength effectiveness ratio of the composite columns. It was also clear that the increase in the thickness of the PVC permanent tube caused an increase in the confined strain to unconfined ratio, thus the confined to the unconfined ratios for the thickness of the PVC tube ranged from (3.7-8.5 mm) were (1-5.540), (1-3.365), and (1-3.06) for C30, C45, and C60 specimens, respectively [6]. Moreover, the ratios of the confined to unconfined strain were 1.163 and 1.217 for LW and RW composite columns [54]. The increase in the slender ratio of composite columns caused an increase in the ratio of confined to unconfined strength as offered in Table 2 [52]. Subsequently, the ratios of confined to unconfined strength ranged from (1.97-1.18) and (2.32-1.3) for 110 mm diameter specimens with slender ratios 2 and 3, respectively. On the other hand, the ratios were (3.04-

1.82), (3.27-1.86), and (3.65-1.92) for 83 mm diameter specimens with slender ratios 2, 3 and 4, respectively. Besides, the ratios were (2.55-1.4), (2.71-1.51), and (2.96-1.83) for 55 mm diameter specimens with slender ratios 2, 3, and 4, respectively.

The confined strengths of concrete-filled CFRP-PVC permanent tube composite columns ranged from (1669.9-1016.5) kN for (3-9) height-to-diameter ratios of the columns [51].

Table 2: Properties of composite column (SIP formwork confined concrete)

Type of SIP formwork	Thickness t (mm)	Cross section dimensions	Specimen	F_{cc} confined strength	F_{uc} unconfined strength	F_{cc}/F_{uc} (Confinement Effectiveness)	$\frac{\epsilon_{cu}}{\epsilon_{uc}}$ confined strain/unconfined	Ref.
CFRP-PVC tubular (CFCT)	CFRP layer 0.17 PVC 4.5	PVC tube (200,600,4.5) external diameter, length, and thickness, respectively	The circular section diameter (D) of paradigms, the thickness of CFRP layer t_f , and the slenderness ratio (λ): $\lambda = \frac{L}{i} = \frac{4L}{D}$ Where: (L, D & i) represent the effective length, the diameter of the specimen, and the radius of gyration, respectively. N_{ue} experimental ultimate load. f_{cu} cube compressive strength of concrete. f_t tensile strength of CFRP. The specimen symbol C, xx, N, n, M & k: grade of concrete, CFRP layers number, and the height-to-diameter ratio of the paradigms, respectively.	(C30N2M3=1669.9) kN (C30N2M5=1540.7) kN (C30N2M7=1413.9) kN (C30N2M9=1016.5) kN				[51]
Unplasticized polyvinyl chloride (UPVC)	2.5, 3, 2.5	UPVC outer diameters: (55,83 and 110) mm with thicknesses (2.5, 3.0, and 2.5) mm, respectively. slender ratio=(2,3 & 4)	Concrete distinguish(dai./slen.), t thickness C20-(110/2)t2.5 C25-(110/2)t2.5 C30-(110/2)t2.5 C20-(110/3)t2.5 C25-(110/3)t2.5 C30-(110/3)t2.5 C20-(83/2)t3 C25-(83/2)t3 C30-(83/2)t3 C20-(83/3)t3 C25-(83/3)t3 C30-(83/3)t3 C20-(83/4)t3 C25-(83/4)t3 C30-(83/4)t3 C20-(55/2)t2.5 C25-(55/2)t2.5 C30-(55/2)t2.5 C20-(55/3)t2.5 C25-(55/3)t2.5 C30-(55/3)t2.5 C20-(55/4)t2.5 C25-(55/4)t2.5 C30-(55/4)t2.5	17.6 MPa 19.1 MPa 20.5 MPa 17.0 MPa 18.1 MPa 19.0 MPa 24.2 MPa 26.0 MPa 26.8 MPa 22.5 MPa 24.6 MPa 25.0 MPa 22.1 MPa 24.1 MPa 24.5 MPa 25.3 MPa 28.4 MPa 29.3 MPa 24.7 MPa 26.9 MPa 27.8 MPa 23.0 MPa 23.2 MPa 26.3 MPa	8.9 MPa 16.0MPa 17.4MPa 7.4 MPa 14.5 MPa 14.6 MPa 8.0 MPa 14.3 MPa 14.7 MPa 6.9 MPa 12.0 MPa 13.5 MPa 6.1 MPa 10.7 MPa 12.8 MPa 9.9 MPa 20.0 MPa 20.9 MPa 9.1 MPa 15.7 MPa 18.4 MPa 7.8 MPa 12.2 MPa 14.4 MPa	1.97 1.20 1.18 2.32 1.25 1.30 3.04 1.82 1.82 3.27 2.05 1.86 3.65 2.24 1.92 2.55 1.42 1.40 2.71 1.72 1.51 2.96 1.91 1.83		[52]
PVC	3.7, 5.2 8.5	PVC outer diameters 110 & length 220 mm. with thicknesses (3.7,5.2 and 8.5) mm	C30 PVC3.7-C30 PVC5.2-C30 PVC8.5-C30 C45 PVC3.7-C45 PVC5.2-C45 PVC8.5-C45 C60 PVC3.7-C60 PVC5.2-C60 PVC8.5-C60	18.20 MPa 30.59 MPa 34.90 MPa 42.68 MPa 27.32 MPa 36.17 MPa 41.26 MPa 45.55 MPa 49.00 MPa 49.54 MPa 49.70 MPa 49.95 MPa	1.000 1.681 1.918 2.345 1.000 1.324 1.511 1.668 1.000 1.011 1.014 1.019	1.000 3.518 3.679 5.540 1.000 2.094 2.484 3.365 1.000 1.415 2.189 3.062	[6]	

Table 2: Continued

Steel tube	3.7, 2.3	Steel tube: (Group-1 i.e., specimen 1-4 Diameter=165.2, thickness=3.7). (Group-2, i.e., specimen 5-6 Diameter=230, thickness=2.3). Entire paradigms were created to own a same length-to-diameter ratio= 3. paradigm-1, $f_c = 29.5$, $\lambda = 1.19$; paradigm-2, $f_c = 43.5$, $\lambda = 0.81$; paradigm-3, $f_c = 58.0$, $\lambda = 0.61$; paradigm-4, $f_c = 81.6$, $\lambda = 0.43$; (E) paradigm-5, $f_c = 32.0$, $\lambda = 0.46$; (F) paradigm -6, $f_c = 64.0$, $\lambda = 0.23$.	The nominal axial power of CFT: $N_0 = f_s A_s + f_c A_c$. F_s : yield power A_s : sectional area of steel tube. F_c : compressive power A_c : sectional area of concrete. confinement factor, $\lambda = \frac{f_s A_s}{f_c A_c}$		Confinement Effect: Figure 1	[53]		
grid-reinforced UHPC concrete	(20 & 40)	Diameter x height: (240 x 600)	RC20 & RC40 are the control specimens for thickness 20, 40 SIP formwork. The letter T L, S, or C indicates formwork thickness (mm); the number of SS grid or CFRP layers.	RC20: 29.3 MPa T20L0: 49.6MPa T20S1: 45.2 MPa T20C1: 53.6MPa RC40: 29.3 MPa T40L0: 84.1MPa T40S1: 85.7 MPa T40S2: 88.8 MPa	- 1.69 1.54 1.83 - 2.87 2.92 3.03	- 0.864 0.822 2.193 - 1.237 1.162 1.332	[49]	
Composite columns : AFS-Logicwall (LW) and AFS-Rediwall (RW). Reference column: Standard columns (STCs) 3D printed-precast permanent concrete formwork.	thickness: (6 & 3) for Fiber cement board (FCB) & PVC, respectively.	AFS- LW (188x600x1200) STC (188x600x1200) AFS- RW (256x600x1200) STC (256x600x1200)	Modulus of elasticity core concrete & FCB: (24 & 5) GPa, respectively.	AFS LW (LW)= 3663 kN AFS RW (RW)= 4069 kN	STC for AFS LW =1.18 (STCL W)= 3109 kN STC for AFS RW (STCR W)= 3843 kN	(LW)=3663\3 109 =1.18 (RW)=4069\3 843 =1.06	(STCLW)=1.163 (STCRW)=1.217	[54]
3D printed-precast permanent concrete formwork.	25 mm	Diameter X length: (250x 600) mm for all columns.	The letters: J0: without reinforcement J1: with reinforcement details; C8@100 mm stirrup & 6 C14 longitudinal bar. J2: with reinforcement details; C8@100 mm stirrup & 8 C14 longitudinal bar. The printed and the core concrete compressive strength: 40 & 30 MPa, respectively. the 0.0%, 0.0%, 1.9%, 1.9%, 2.5% and 2.5% were reinforcement ratios for the 3DP-PJ0, Cast-PJ0, 3DP-PJ1, Cast-PJ1, 3DP-PJ2 and Cast-PJ2 paradigms, respectively.	3DP-PJ0 1700 KN 3DP-PJ1 2025 KN 3DP-PJ2 2240 KN	CastPJ0 1450 KN CastPJ1 1750 KN CastPJ2 1950 KN		[55]	

3. Compressive Strength and Confined Effect

The researchers demonstrated the behavior of concrete-filled CFRP-PVC composite columns as indicated in Table 2. Jiang et al. [51], cleared that there was a reduction in the ultimate load with the rising slenderness ratio due to the instability of the failure pattern of columns. Moreover, the outcomes of the study elucidated that the load-deflection curves coincided with each other before the crushing of core concrete which could be due to the non-activation of restraining of CFRP-PVC tubes yet as the core concrete is in an elastic stage [51].

Oyawa et al. [52], investigated the behavior of concrete-filled SIP plastic tubes under compressive load. It was found that plastic pipes were gorgeous in concrete restriction by the raised compressive stress of confined paradigms. The strength was enhanced from 1.18 to 3.65 times the non-restriction strength related to the restriction level.

3.1 Effect Thickness of SIP Formworks

From Table 2 and Table 3, it was clear that the increase in the pipe thickness caused an increase in the ultimate strength and SI (confined ratio= f_{cc}/f_{c}) of the composite columns with C30 and C45. The composite columns with C60 slightly varied in the ultimate strength and SI with the boost of pipe thickness [6].

The explanation for this behavior was that the confined and unconfined specimens had the same size. Therefore, the PVC pipe in the confined specimen could be considered to replace a concrete pipe with the same thickness. Moreover, the ultimate load capacity of the confined specimen (N_p) equals the ultimate load capacity of the unconfined specimen (N_c) plus the increase in the ultimate capacity of the confined specimen due to the strengthened effect of PVC pipe confinement (P_{confined}) plus the difference between PVC pipe and concrete pipe in ultimate capacity (ΔN). N_{confined} was a positive value, while ΔN could be a positive or negative value. Therefore, the confined specimens increased with the thickness of the PVC confined tube increased.

It was also clear that the composite columns had a higher maximum load and elastic modulus than the normal control columns. Thus, the increase in thickness of SIP formwork caused the boost in maximum load and elastic modulus. However, there was a more considerable abrupt strength loss promptly after the initial peak load for the thicker UHPC formwork without lateral restrain paradigms (i.e., specimens without CFRP or SS grids). Although a thinner formwork had a strong recovery due to the bond strength between the UHPC matrix and steel fibers, this behavior was not noticed in paradigms with thicker formwork. Therefore, the ductility and toughness indexes diminished due to the UHPC material's brittle matter [49].

Oyawa et al. [52], investigated the behavior of concrete-filled SIP plastic tubes under compressive load and the restriction effect increased with the rising of plastic tube thickness; thus, a confinement matter depended on the radial stiffness of a restriction member to confine the expansion as shown in Table 2.

Table 3 shows that the best-affected thickness for uPVC-SIP formwork composite columns was 3mm, as a 0.5mm increase in SIP formwork thickness caused an increase in composite column strength of more than 60%. At the same time, the more effective thickness for PVC-SIP formwork was 5.3mm because a 3.3mm increase in the thickness of the SIP formwork caused an increase in composite column strength of not more than 40%.

Liu et al. [56] demonstrated the axial compressive behavior of concrete-filled square steel tube stub columns; their study results are presented in Table 4. It was clear from Table 4 that the increase in steel tube led to an increase in the ultimate strength of composite columns, and the most effective thickness was 4.5 mm because the increase in thickness of only 0.75 mm led to double the increase in strength present.

The restriction influence of various strengths of classes of concrete-filled steel tube columns was demonstrated by He et al. [53]. The confined pressure finally rose from zero to a closely steady enduring value. The mysterious concrete power is enhanced with the improvement in reserved pressure. The higher the restriction factor value ($\lambda = fsAs / fcAc$) the higher the restriction pressure, as shown in Figure 1.

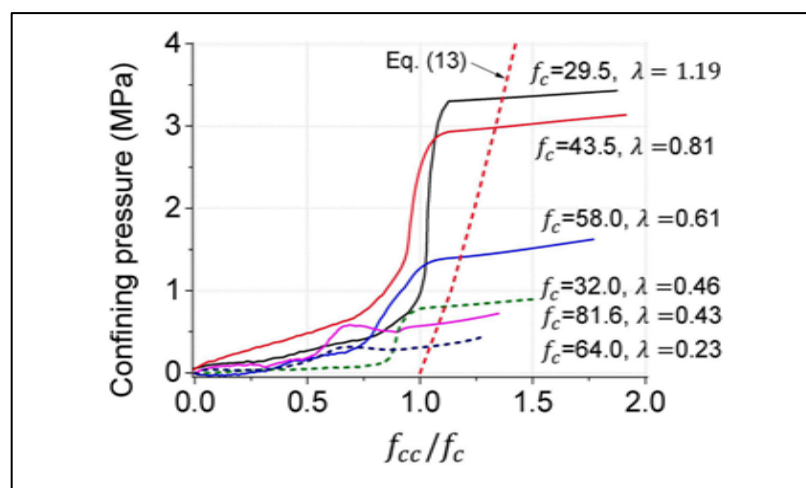


Figure 1: Relationship between confined concrete power and confining pressure [53]

Shen et al. [57], studied the axial compressive behavior of rubberized concrete-filled steel tube short columns (RuCFST). It was found that the axial compressive capacity of the columns decreased with the increase in the volume of the rubber replacement ratio (R). On the other hand, the strength reduction of RuCFST columns with larger steel tube thicknesses was much less pronounced than that of RuCFST columns with smaller steel tube thicknesses due to the contribution of the steel tube to the overall columns' resistance and concrete confinement [57].

Kildashti et al. [58], employed the FE numerical model to investigate the impact of the FCB thickness on the axial load–displacement attitude of AFS-LW paradigms. The FCB-FE model thickness ranged from 12 to 24mm, while the control FCB model thickness was 6mm. There was a tenuous contribution in the initial axial stiffness of AFS-LW paradigms with the progressing thickness of FCB. At the same time, the rising of the FCB thickness caused a middle improvement in the ultimate axial power of the samples. Moreover, the impact of PVC encasement thickness on the axial behavior of AFS-RW paradigms was inspected by varying the thickness from 3, 6, and 12mm [54]. It was also obvious that the primary axial stiffness of the AFS-RW paradigms was unmodified. On the other hand, the improvement in the axial capping load was 6.9%, with the progress of a PVC thickness from 3mm to 12mm. Moreover, the axial ductility factor of the AFS-RW paradigm was also improved with rising PVC thickness. Meng and Khayat [58], developed 12 cases of prefabricated UHPC reinforced with embedded GFRP grids SIP formwork for concrete columns by using the finite element analysis software ABAQUS as presented in Table 5. It was found that the maximum principal stress decreased with the SIP formwork thickness increase, as offered in Figure 2.

Table 3: Effect thickness of SIP formwork on compressive strength of composite columns

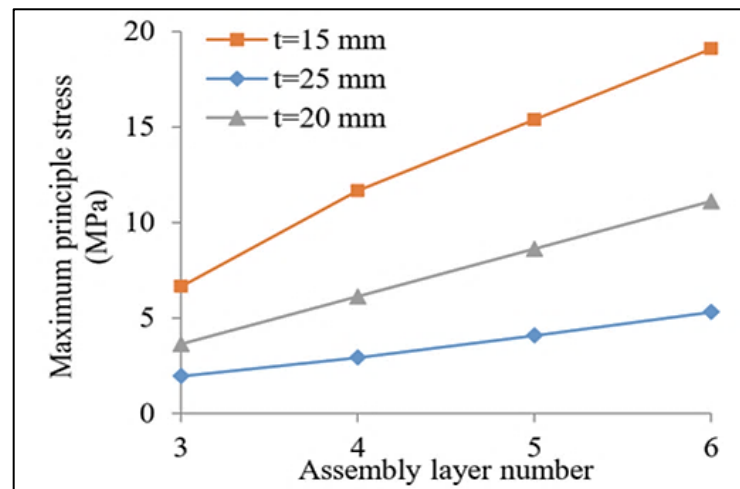
Type of SIP formwork	Compressive strength of concrete	Thickness of SIP formwork (mm)	Increase in strength % from control column	Ref.		
PVC	Core concrete= C30 (34.9 MPa)	0	Control	[6]		
		3.7	68.077			
		5.2	91.758			
	Core concrete= C45 (58 MPa)	8.5	134.505			
		0	Control			
		3.7	32.394			
	Core concrete= C60 (74.9 MPa)	5.2	51.025			
		8.5	66.728			
		0	Control			
		3.7	1.102			
		5.2	1.429			
		8.5	1.939			
uPVC	Core concrete= C20 (20.7 MPa)	0	Control	[52]		
		2.5	97.753			
		3	202.5			
	Core concrete= C25 (27.2 MPa)	0	Control			
		2.5	19.375			
		3	81.818			
	Core concrete= C30 (30.7 MPa)	0	Control			
		2.5	17.816			
		3	82.313			
	grid-reinforced UHPC concrete	Core concrete= 32.4 MPa UHPC-SIP concrete=139.3 MPa	0		Control	[49]
			20		69.283	
			40		187.031	
Steel tube	Core concrete= C40 (40 MPa)	3	Control	[56]		
		3.75	4.762			
		4.5	15.646			
Steel tube	Core concrete= C50 (50 MPa)	3	Control			
		3.75	10.625			
		4.5	31.25			
Steel tube	Core concrete= C60 (60 MPa)	3	Control			
		3.75	15.976			
		4.5	26.627			

Table 4: Axial Behavior of Concrete-filled Square Steel Tube Stub Columns [56]

Specimens	Compressive strength of core concrete (MPa)	Thickness of steel tube, (mm)	Ultimate strength of composite column (N_u), (kN)	Ultimate displacement of composite column (Δ_u), (mm)	Displacement at $0.85*N_u$ in descending part of the load-displacement curve ($\Delta_{0.85}$), (mm)	Ductility index (DI)
C40-t3	40	3	1470	3.20	5.56	1.74
C40-t3.75	40	3.75	1540	3.41	7.10	2.08
C40-t4.5	40	4.5	1700	3.26	8.70	2.67
C50-t3	50	3	1600	3.02	4.87	1.61
C50-t3.75	50	3.75	1770	3.17	5.80	1.83
C50-t4.5	50	4.5	2100	3.51	8.22	2.34
C60-t3	60	3	1690	2.57	4.50	1.75
C60-t3.75	60	3.75	1960	2.95	5.01	1.70
C60-t4.5	60	4.5	2140	3.30	7.22	2.19

Table 5: Investigated cases [58]

Cases	Assembly layer number	SIP formwork thickness
1-3	3	15, 20, 25
4-6	4	15, 20, 25
7-9	5	15, 20, 25
10-12	6	15, 20, 25

**Figure 2:** Effects of assembly layer number and SIP formwork thickness on maximum principal stress [58]

3.2 Effect of Strength Grade of Core Concrete

It is clear from Table 6 that the increase in the core strength of approximately 20 MPa led to double the increase in the strength percent of a composite column for the PVC-SIP formwork specimen. On the other hand, the increase in the core strength of approximately 3 MPa led to double the increase in the strength percent of a composite column for uPVC-SIP formwork specimens. Moreover, it was found that the restriction effectiveness descended with the rise of the restriction strength of concrete. This behavior could be because of more brittleness and less expansion for the higher-strength concrete [52]. It can be concluded from Table 6 that the core concrete is the major member to carry the axial load of composite columns as the increase in strength core grade led to a noticeable increase in the ultimate strength of the maximum compression load of the composite column could be achieved with a circular cross-section for plastic or steel SIP formwork the maximum compression load of the composite column could be achieved with a circular cross-section for plastic or steel SIP formwork the composite column. It was also clear that the most effective strength grade of core concrete to be confined by steel tube was 50 MPa because of giving the maximum increase in ultimate load of the composite column, which was 27.273 [56]. Increasing the compressive strength of the concrete core caused improvement in the axial performance of CFST columns. Furthermore, the effect for specimens with a square cross-section shape was higher than those with circular and octagonal shapes [59].

He et al. [53] demonstrated the restriction influence of various strength classes of concrete-filled steel tube columns. Obviously, for paradigms with similar restriction factors ($\lambda = A_{sfs}/A_{cfc}$), such as paradigms 4 and 5, the smaller concrete strength paradigms offered a lower decline in axial strength than that of higher concrete strength. In other words, paradigm 5 had a smaller decline in axial strength than paradigm 4. The details of the paradigms and strengths are presented in Table 7 [53]. Rong et al. [60], studied the axial compression behavior of concrete-filled aluminum tubular columns; the study details are offered in Table 8. It was found that the confinement effect of the aluminum alloy outer tube on the core concrete gradually strengthened with the load growing, and the specimen's lateral strains were dramatically deformed, indicating an aluminum alloy outer tube with excellent ductility. A similar behavior was demonstrated by Yan et al. [61] as explained in Table 9.

Numerical FE analyses on AFS-encased columns organized by concrete with several compressive strengths ranging from 20 MPa to 50 MPa were conducted by [54]. The study's outcomes introduced an improvement in the primer axial stiffness and the ultimate axial capacity of axial load-displacement curves for each of the AFS-encased paradigms and the corresponding STCs with higher strength concrete. Besides, for the paradigms with the same concrete strength, the AFS-LW paradigm established a moderate rise in axial stiffness compared to the STC rival. In contrast, the axial capping loads were introduced to be substantially enhanced using the AFS-LW encasement. Also, the results clarified a slight advancement in the maximum axial capacity of paradigms with PVC encasements compared to STCs for the entire range of concrete compressive strengths. To sum up, it is clear that the confinement ratio declined with the increase in core concrete strength for almost all types of SIP formwork composite columns, as shown in Figure 3.

Table 6: Effect of core compressive strength grade on compressive strength of composite columns

Cross-section shape	Type of SIP formwork	Thickness of SIP formwork (mm)	Compressive strength of core concrete	Increase in strength %	Ref.			
Circular	PVC	3.7	C30 (34.9 MPa)	Control	[6]			
			C45 (58 MPa)	18.241				
			C60 (74.9 MPa)	61.948				
	5.2	C30 (34.9 MPa)	Control					
		C45 (58 MPa)	18.223					
		C60 (74.9 MPa)	42.407					
	8.5	C30 (34.9 MPa)	Control					
		C45 (58 MPa)	6.724					
		C60 (74.9 MPa)	17.034					
Circular	uPVC	2.5	C20 (20.7 MPa)	Control	[52]			
			C25 (27.2 MPa)	8.523				
			C30 (30.7 MPa)	16.477				
		3	C20 (20.7 MPa)	Control				
			C25 (27.2 MPa)	7.438				
			C30 (30.7 MPa)	10.744				
		Square	Steel tube	3		C40 (40 MPa)	Control	[56]
						C50 (50 MPa)	8.844	
						C60 (60 MPa)	14.966	
3.75	C40 (40 MPa)			Control				
	C50 (50 MPa)			14.935				
	C60 (60 MPa)			27.273				
4.5	C40 (40 MPa)			Control				
	C50 (50 MPa)			23.529				
	C60 (60 MPa)			25.882				
Square	Steel tube	8	30S (40 MPa)	Control	[59]			
			50S (85 MPa)	41.549				
			80S (120 MPa)	74.12				
		Circular	30C (40 MPa)	Control				
			50C (85 MPa)	27.18				
			80C (120 MPa)	45.409				
		octagonal	30O (40 MPa)	Control				
			50O (85 MPa)	30.362				
			80O (120 MPa)	52.742				

Table 7: Summary of test specimens [53]

Specimen	(D), mm	(t), mm	D/t	Strength of unconfined concrete (f_c) N/mm ²	Strength of steel tube (fs)N/mm ²	($\lambda = f_s A_s / f_c A_c$)	N_0 , kN ($N_0 = f_s A_s + f_c A_c$)	Max. normalized axial strength (N_u)/nominal axial strength (N_0)
1	165.2	3.7	44.6	29.5	366	1.19	1264	1.13
2	165.2	3.7	44.6	43.5	366	0.81	1538	1.09
3	165.2	3.7	44.6	58	366	0.61	1821	1.15
4	165.2	3.7	44.6	81.6	366	0.43	2283	1.1
5	230	2.3	100	32	360.8	0.46	1870	1.06
6	230	2.3	100	64	360.8	0.23	3147	1.04

Table 8: Specimen details and test results of concrete-filled aluminum tube composite column [60]

Specimen	Specimen height, (L), mm	Specimen diameter, (D), mm	Tube thickness, (t), mm	Slender ratio (λ)	Compressive strength of core concrete, MPa	Ultimate load of composite column, kN
C-345-70-1	345	70	5	19.71	47.6	695.6
C-345-70-2	345	70	5	19.71	49.1	719.4
C-370-75-1	370	75	5	19.73	50.7	730.2
C-370-75-2	370	75	5	19.73	51.8	753.1
C-810-70-1	810	70	5	46.28	46.4	476.7
C-810-70-2	810	70	5	46.28	48.8	490.3
C-870-75-1	870	75	5	46.4	50.2	508.7
C-870-75-2	870	75	5	46.4	47.2	522.5
C-1270-70-1	1270	70	5	72.57	49.5	243.2
C-1365-75-2	1365	75	5	72.8	45.7	294.6

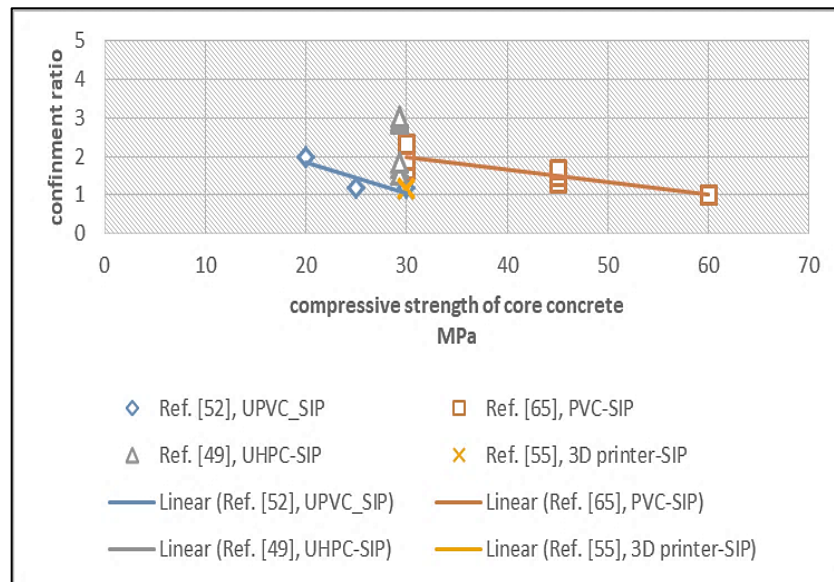


Figure 3: Compressive strength VS. Confinement ratio for some SIP formwork composite columns

Table 9: Specimen details and test results of concrete-filled aluminum tube composite column [61]

Specimen	Specimen diameter, (D), mm	Tube thickness, (t), mm	Compressive strength of core concrete, MPa	Specimen height, (L), mm	Ultimate load of the composite column, numerical, kN
G1-D180	180	9.00	75	540	3069
G1-D300	300	9.00	75	900	6906
G1-D420	420	9.00	75	1260	11,405
G1-D540	540	9.00	75	1620	18,239
G2-T17.5	350	17.50	80	1050	11,472
G2-T10.6	350	10.60	80	1050	9705
G2-T7.4	350	7.40	80	1050	8742
G2-T5.8	350	5.80	80	1050	8043
G3-A110	250	6.25	70	750	3431
G3-A160	250	6.25	70	750	3770
G3-A240	250	6.25	70	750	4306
G3-A345	250	6.25	70	750	5006
G4-A110	450	7.50	70	1350	10,251
G4-A160	450	7.50	70	1350	10,897
G4-A240	450	7.50	70	1350	12,043
G4-A345	450	7.50	70	1350	13,410
G5-CON50	250	5.00	50	750	3318
G5-CON70	250	5.00	70	750	4104
G5-CON90	250	5.00	90	750	4887
G5-CON110	250	5.00	110	750	5668
G6-CON50	480	8.00	50	1440	10,868
G6-CON70	480	8.00	70	1440	13,702
G6-CON90	480	8.00	90	1440	16,540
G6-CON110	480	8.00	110	1440	19,379

3.3 Effect of Cross-Section Shape of The Composite Column

It was clear from Table 10 that the composite column's maximum compression load, the maximum compression load of the composite column could be achieved with a circular cross-section for plastic or steel SIP formwork. This behavior could be attributed to the confinement effect, which is more effective with a circular cross-section shape. Moreover, it was clear from Table 2 that restriction effectiveness declined with the rise in the slenderness ratio. This conduct could be due to the columns' reduced load-carrying capacity with an increased and decreased slenderness ratio [52]. Pour et al. [59], investigated the effect of cross-section shape on compressive behavior on concrete with different strength grade filled steel tubes; their study details are presented in Table 11. Moreover, it was clear from Table 11 that there was a similar behavior a similar behavior was explained above. Thus, the circular cross-section shape had a maximum load-carrying capacity, followed by octagonal and square shapes, respectively.

Table 10: Effect of cross-section shape of SIP formwork composite columns on compressive behavior

Type of SIP formwork	Cross-section shape	Cross-section dimension of column (mm)	Maximum load, (kN)	Ref.	
3-D printed plastic	Square	Area (A)= 266.2 mm ² Internal circumference (P) = 160.0 mm	41	[62]	
	Circle	A= 141.8 mm ² P= 234.9 mm	53		
	Pentagon	A= 252.3 mm ² P= 152.4 mm	40		
	2nd iteration of Ceasaro Polyflake	A= 376.3 mm ² P= 232.8 mm	40		
	3rd iteration of Ceasaro Polyflake	A= 558.8 mm ² P = 355.1 mm	40		
	3rd iteration of the Koch Star	A= 425.2 mm ² , P= 263.4 mm,	40		
	Area				
	4th iteration of the Koch Star	A=521.4 mm ² P=336.4 mm	40		
Steel tube	Circular (CC)	P= 503 mm, A=20106 mm ²	744.9	[63]	
	Square (CS)	P=500 mm A=15625 mm ²	668.9		
	Square with rounded-ended (CSE)	P=500 mm A=15625 mm ²	694.9		
	Rhombic (CRH)	P=500 mm A=15000 mm ²	629.3		
	Rectangular (CR)	P=510 mm A=14450 mm ²	605.2		
	Rectangular with round-ended (CRE)	P=506 mm A=15903 mm ²	621.8		
	Elliptical (CE)	P=484 mm A=15708 mm ²	607.4		
	Hexagonal asymmetric (CHA)	P=500 mm A=16500 mm ²	565.9		
	Triangle (CT)	P=510 mm A=12512 mm ²	491.8		
	Pentagram (CP)	P=500 mm A=17205 mm ²	669.7		
	Hexagon (CH)	P=510 mm A=18771 mm ²	703.1		
	Octagon (CO)	P=480 mm A=17382 mm ²	760.3		
	1/4 circular (CQC)	P=500 mm A=15394 mm ²	596.7		
	Semi-circular (CSC)	P=514 mm A=15708 mm ²	554.1		
	D-Shaped (CD)	P=500 mm A=15735 mm ²	547.2		
	Fan-shaped (CF)	P=500 mm A=16897 mm ²	577.7		
	L-Shape (CL)	P=520 mm A=12675 mm ²	530.7		
	T-Shape (CTS)	P=500 mm A=10000 mm ²	475.4		
	Plus-shaped (CPS)	P=480 mm A=8000 mm ²	490.6		
	Square	Length of one side=200 mm	30S= 6816.0 50S= 9648.0 80S=11,868.0		
	Circular	Diameter=280 mm	30C=13,472.0 50C=17,133.8 80C=19,589.5		
	Octagonal	Diameter=250 mm Length of one side=105 mm	30O=10,618.4 50O=13,842.4 80O=16,218.8		

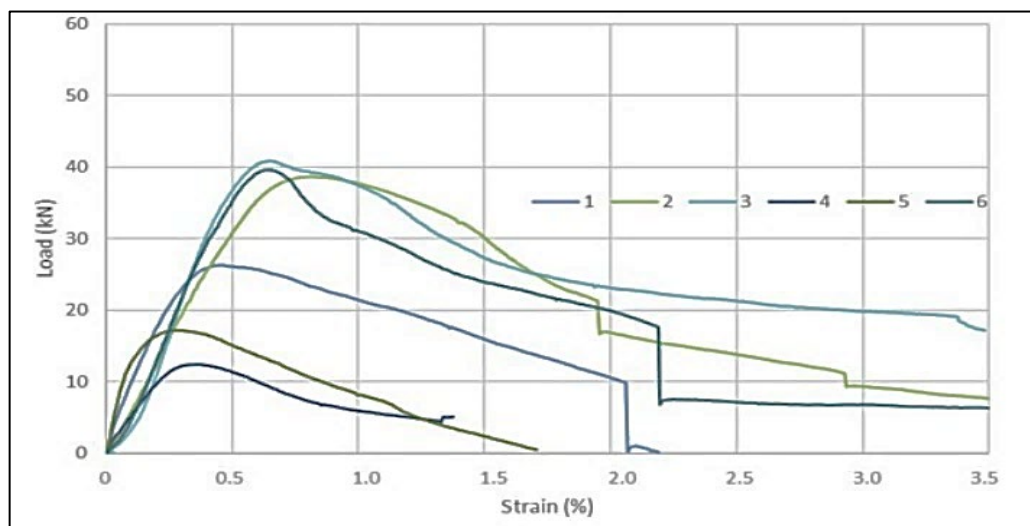
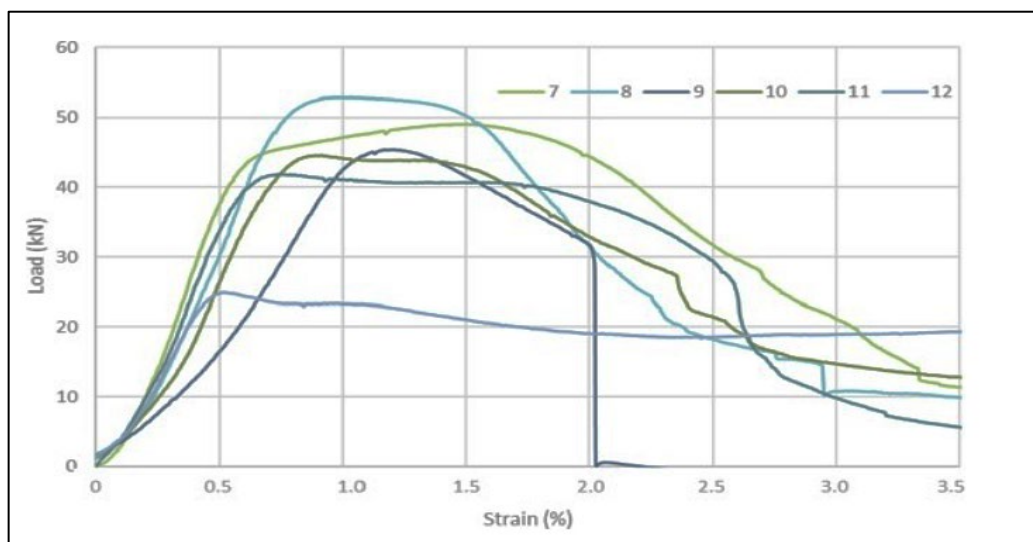
Table 11: Specimen details and compressive behavior of concrete-filled steel tube composite columns [59]

Specimen	Cross-section shape	Compressive strength of core concrete, (MPa)	Thickness of steel tube, (mm)	Confined compressive load, kN (N_u)	Unconfined compressive load, kN (N_P)	N_u/N_P
30C	Circular	40	8	13,472.0	7112.68	1.89
50C	Circular	85	8	17,133.8	10,351.80	1.66
80C	Circular	120	8	19,589.5	12,291.61	1.59
30S	Square	40	8	6816.0	3805.83	1.79
50S	Square	85	8	9648.0	4565.38	2.11
80S	Square	120	8	11,868.0	5705.66	2.08
30O	octagonal	40	8	10,618.4	5974.62	1.78
50O	octagonal	85	8	13,842.4	8603.64	1.61
80O	octagonal	120	8	16,218.8	9777.52	1.66

A sudden drop in the loading force with square cross-sections, as presented in Figure 4, appeared after reaching a strain of 2%, representing such failure. Katzer and Skoratko [62]. On the other hand, only one specimen (no. 9) exhibited instant failure of the plastic formwork with a circular cross-section, as presented in Figure 5.

Relations registered for specimens with pentagon cross-sections, as offered in Figures 6 and 7, were similar to those registered for specimens with circular cross-sections. One specimen was characterized by instant failure of the plastic formwork (no. 14). Besides, load-strain relations for all other specimens represent similar behavior and form a much tighter family of results than specimens with circular and square cross-sections.

All tested specimens with fractal-based cross-sections were characterized by highly quasi-plastic behavior, as presented in Figures (8–10). After reaching the ultimate loading force, the subsequent destruction process was smooth (without sudden plastic breaking) and accompanied by large horizontal deformations of the formwork.

**Figure 4:** Load–deflection relations of square composite columns (specimens from 1 to 6) [62]**Figure 5:** Load–deflection relations of circular composite columns (specimens from 7 to 12) [62]

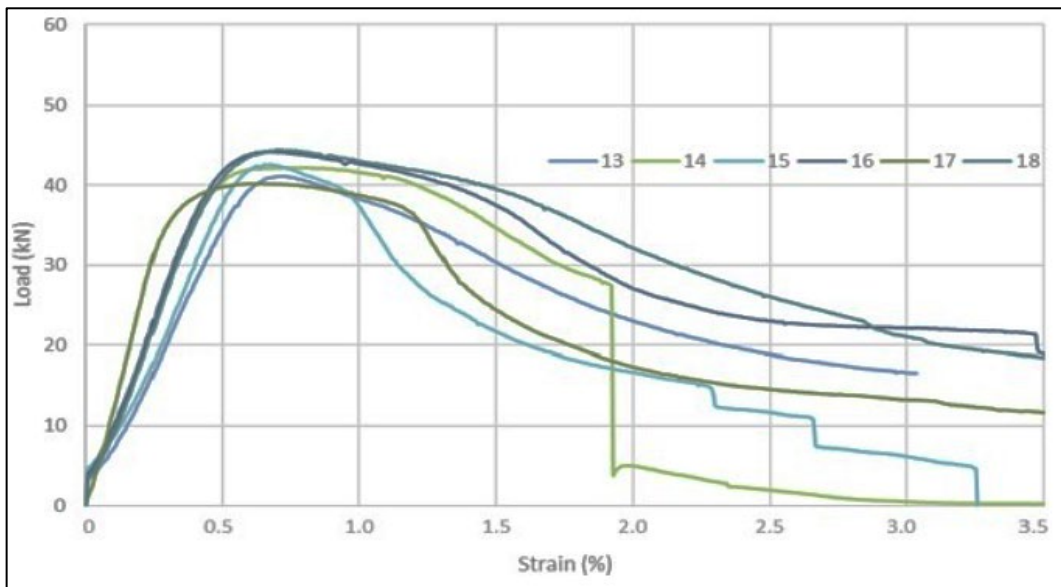


Figure 6: Load–deflection relations of pentagon shape composite columns (specimens from 13 to 18) [62]

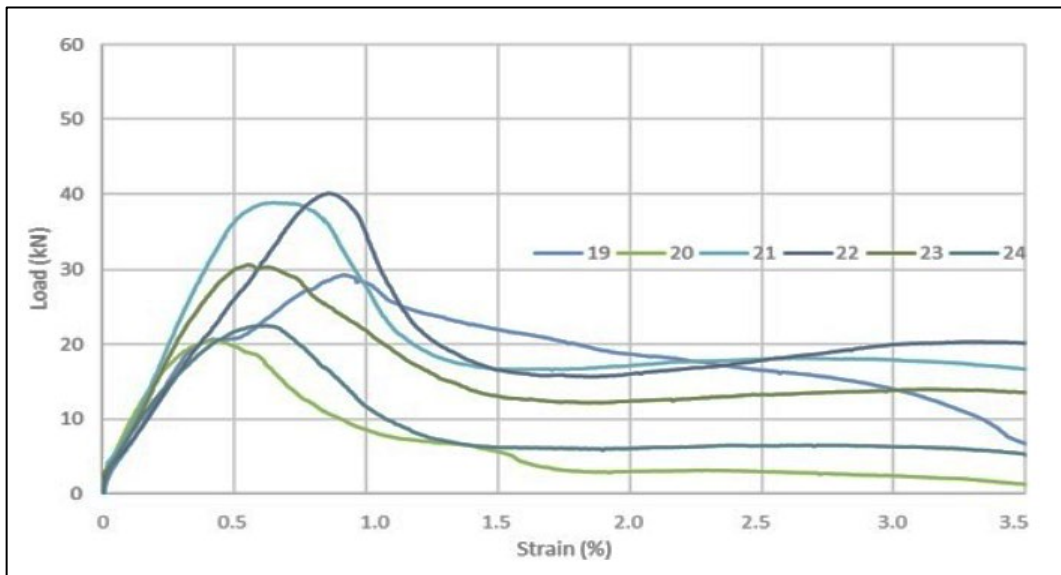


Figure 7: Load–deflection relations of the second iteration of the Ceasaro Polyflake shape composite columns (specimens from 19 to 24) [62]

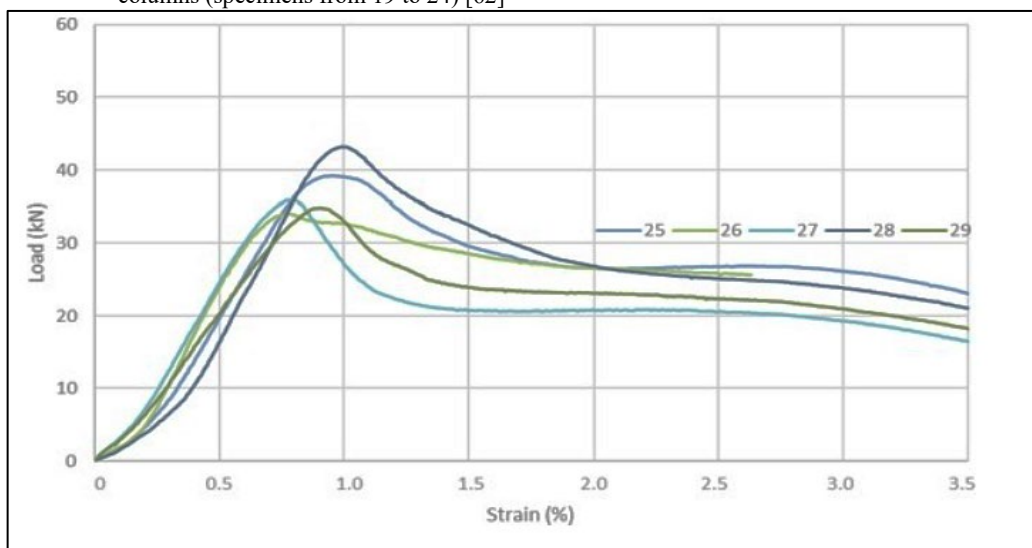


Figure 8: Load–deflection relations of the third iteration of the Ceasaro Polyflake shape composite columns (specimens from 25 to 29) [62]

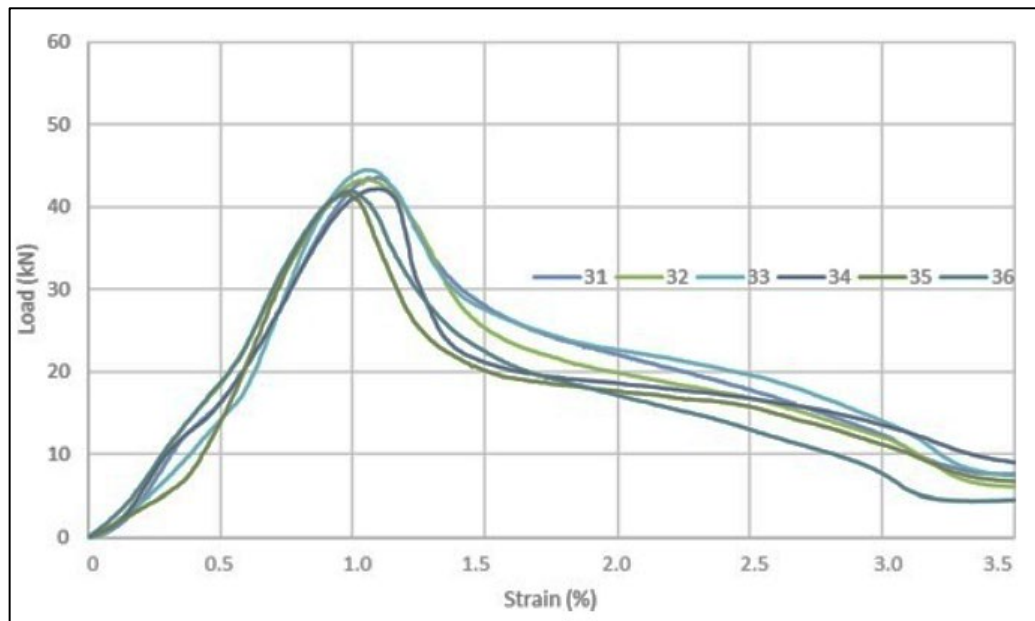


Figure 9: Load–deflection relations of the third iteration of the Koch Star shape composite columns (specimens from 31 to 36) [62]

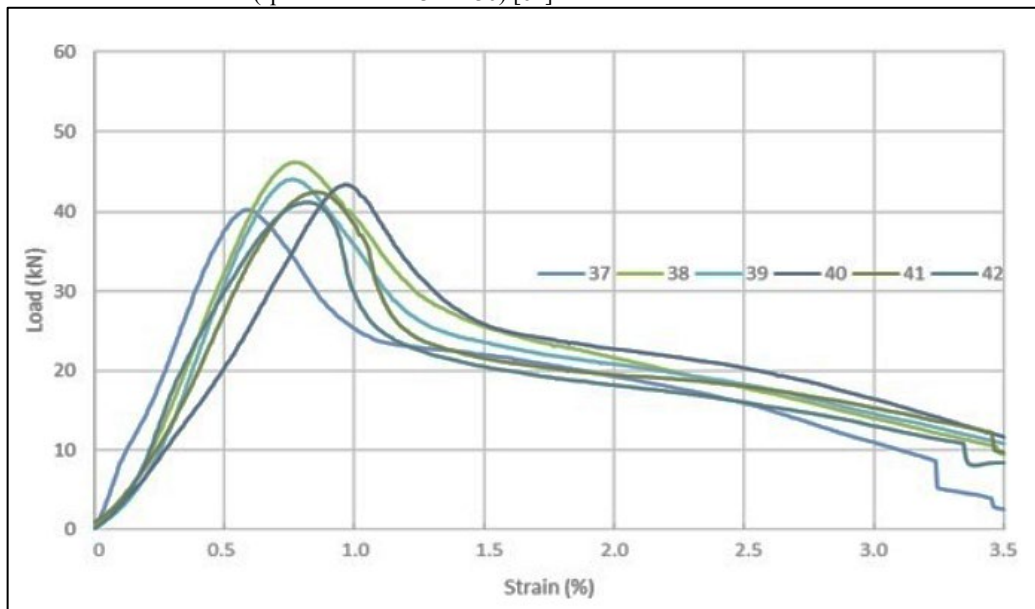


Figure 10: Load–deflection relations of the fourth iteration of the Koch Star shape composite columns (specimens from 37 to 42) [62]

The maximum compressive strengths of different shapes of composite columns are presented in Figure 11. Moreover, the strengths were calculated according to areas of core concrete and plastic formwork (ASFRC+ABS) and according to the area of core concrete (ASFRC) [62]. It was noticed that taking into account the cross-sectional area of plastic formwork was especially influential in the case of fractal-based cross-sections. Thus, the differences in the case of the 4th iteration of the Koch Star cross-section reached the value of 6.6 MPa.

The results in Table 10 show that the ultimate stress of the specimens with Octagon (CO) columns was about 14% higher than that of the circular column. Furthermore, it was found that sections of Octagon (CO) and Plus-Shaped (CPS) sections appeared to have higher failure stress than those of D-Shaped (CD) and Hexagonal Asymmetric (CHA) [63].

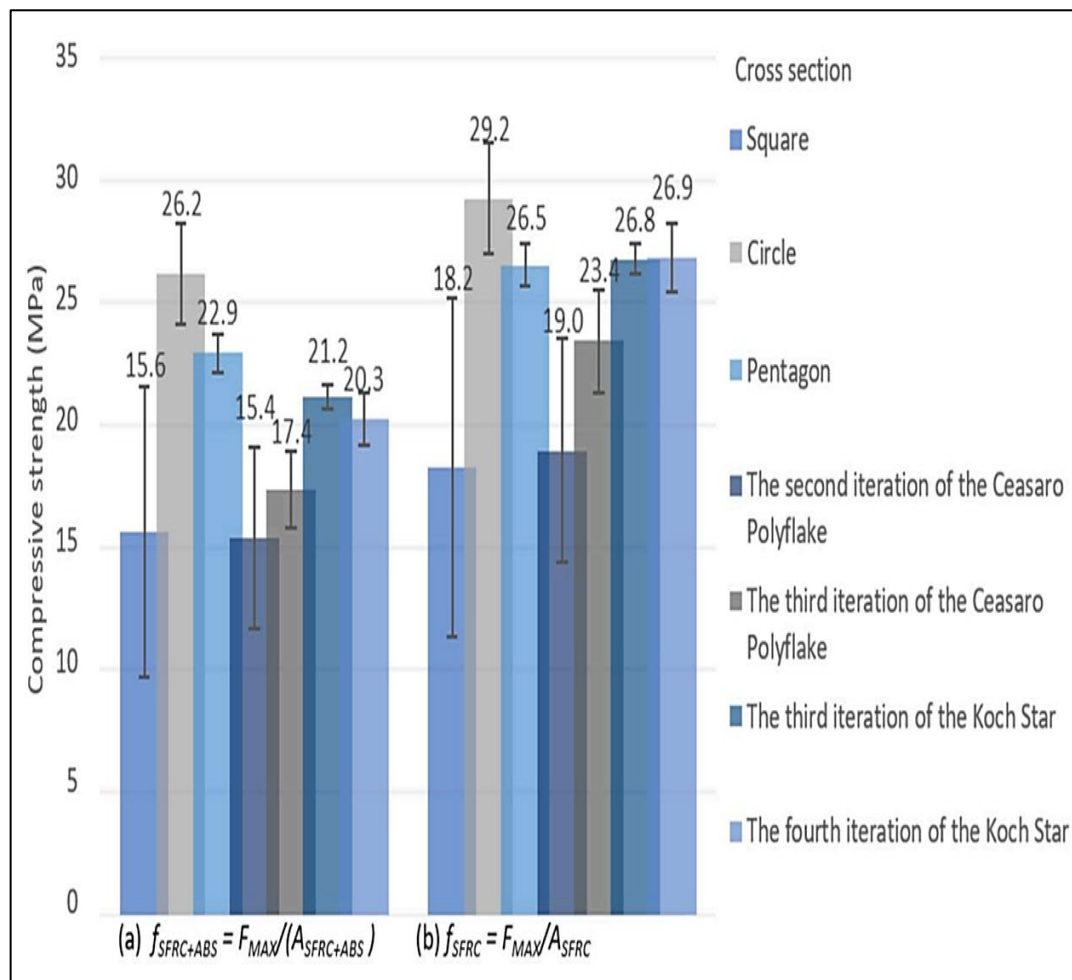


Figure 11: Compressive strength of different cross-section shapes of composite columns [62]

4. Modes of Failure

From Table 12, most of the deterioration of concrete-filled plastic tubes occurred from the mid-height to the quarter-height of the tube of the paradigm with the concrete cracked. In contrast, the C30N2M9 paradigm deteriorated at the column's terminus without the obvious cracks in the core concrete. This behavior may have resulted from more apparent initial eccentricity at a higher slenderness ratio of columns, which was in agreement with Oyawa et al. [52] that they concluded that the ductility had an inverse relationship with a slender ratio of the composite column. Moreover, the hoop strain of composite columns increased at the terminus of the elastic loading stage of the core concrete [51].

There were two categories of failure styles of TPCC paradigms as shown in Table 12:

- 1) Shear-type failure which occurred at the weak confinement by the pipe, led to the damage of core concrete in one direction by shear stress.
- 2) Drum-type failure in which the sample seemed to be like a drum due to the strong pipe constraint; also, in this failure type, there was not a single-direction crack in the core concrete [6].

All specimens (steel tube confined concrete) presented in Table 13 displayed similar failure styles, like buckling the steel tube to the outward direction at both terminuses of high axial lessening and uninterrupted extension at the mid-height. The paradigms with high-power core concrete offered an unmistakable mark of concrete cracking at the mid-height, which clarified the brittle trait of the high-strength concrete [53,57]. On the other hand, the local buckling and shear slip lines constituted a shear failure plane, dividing the specimen into two parts for a concrete-filled square steel tube stub column [56].

Several slant main crushes clarified the failure styles of the concrete-filled UHPC SIP formwork columns, and the completeness of the paradigms was entirely kept because of the excellent bond strength between matrix and steel fibers. On the other hand, the failure modes of RC (normal column without SIP formwork) were clarified by large-area cover spalling [49], as shown in Table 14.

It was also clear from Table 14 that the failure of the columns was brittle. However, it could be concluded that the 3D concrete printer's permanent formwork, compared with a normal column (column without SIP formwork), delays the first crack's appearance even if the core concrete column was not reinforced. Moreover, there was no peeling failure at the formwork's printing interval, which indicated the equality of the stress at the interval and other parts of the composite column. In other words, the composite column had perfect integrity [55].

Table 12: Mode of failure of Plastic-SIP formwork composite columns


Type of SIP-formwork	Mode of failure image	Ref.
CFRP-PVC	 <p>(a) C30N2M3 (b) C30N2M5 (c) C30N2M7 (d) C30N2M9</p>	[51]
UPVC	 <p>(a) Shearing (b) Mid-height bulging (c) Top bulging (d) Bursting (e) Local buckling of empty tubes</p>	[52]
PVC	 <p>(a) Shear-type failure (b) Drum-type failure</p>	[6]

Table 13: Mode of failure of Steel-SIP formwork composite columns

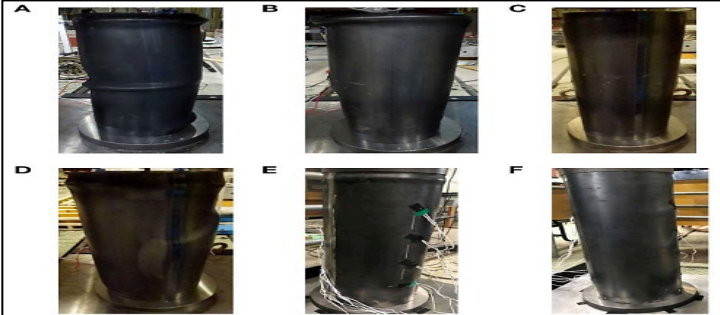
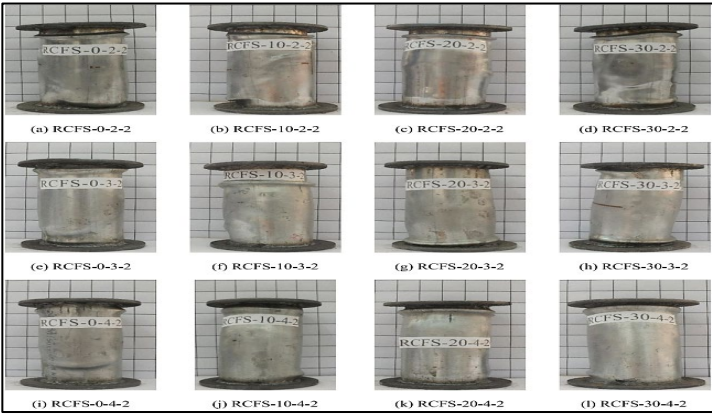

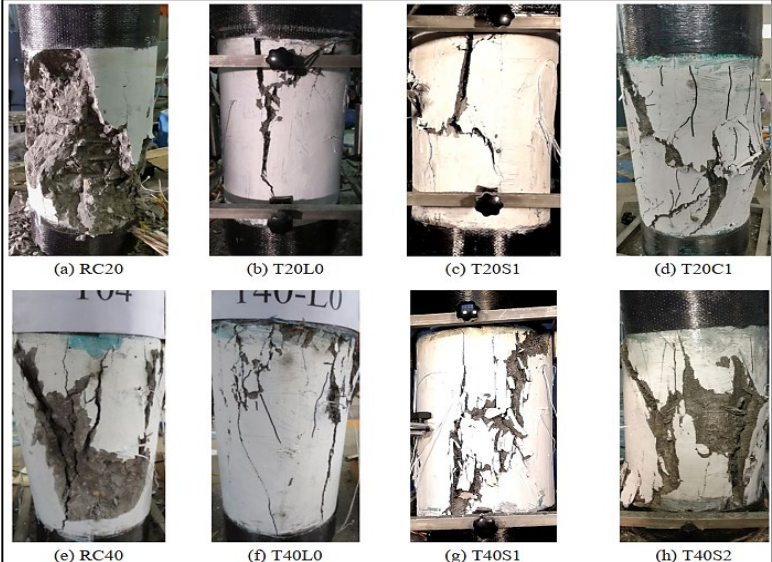
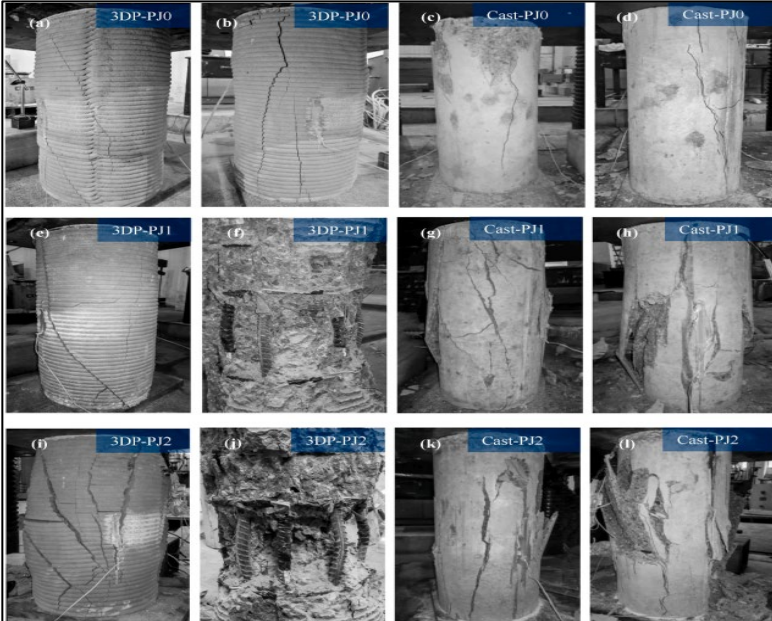
Type of SIP-formwork	Mode of failure image	Ref.
Steel tube		[53]
Steel tube	 <p>(a) RCFS-0-2-2 (b) RCFS-10-2-2 (c) RCFS-20-2-2 (d) RCFS-30-2-2 (e) RCFS-0-3-2 (f) RCFS-10-3-2 (g) RCFS-20-3-2 (h) RCFS-30-3-2 (i) RCFS-0-4-2 (j) RCFS-10-4-2 (k) RCFS-20-4-2 (l) RCFS-30-4-2</p>	[57]
Steel tube		[56]

Table 14: Mode of failure of Concrete-SIP formwork composite columns

Type of SIP-formwork	Mode of failure image	Ref.
UHPC		[49]
3D concrete printer		[55]

5. Ductility

The ratio of the confined strain to the unconfined strain $\epsilon_{cu} \setminus \epsilon_{uc}$ is presented in Table 2. It was clear from Table 2 that the ductility of composite members (concrete-filled SIP formwork) was improved with increasing plastic tube thickness (PVC, uPVC). The same behavior was for other types of SIP formwork like CFRP and steel, as presented in Tables (15-17). On the other hand, from Table 17, it was clear that the ductility index decreased with an increase in UHPC-SIP formwork thickness. In other words, the more brittle composite columns were the thicker UHPC formwork unless lateral restriction for UHPC formwork was supplied, which could be related to the bond strength between the UHPC matrix and steel fibers. Thus, this bond strength was smaller in thicker formwork samples [49]. Also, it was clear that the composite members (concrete-filled SIP formwork members) had more ductility than ordinary members with the exact dimensions and reinforcement ratios (without SIP formwork) for all types of SIP formwork [6,49,51-54].

Table 15: Effect of plastic-SIP formwork on the ductility of composite columns

Type of SIP formwork	specimen	Core concrete strength, MPa	Thickness of plastic tube, (mm)	Ductility index	Ref.
UPVC	C40-3.01	C40	3.01	1.09	[39]
	C40-4.90	C40	4.90	1.18	
	C50-3.27	C50	3.27	1.06	
	C50-4.5	C50	4.5	1.19	
CFRP	CEBR1	-	0.332	2.88	[64]
CFRP	SF1	56.2	0.167	3.48	[65]
	SF1	56.2	0.167	4.37	

Table 16: Effect of steel-SIP formwork on the ductility of composite columns

Type of SIP formwork	specimen	Core concrete strength, MPa	Thickness of plastic tube, (mm)	Ductility index	Ref.
Steel tube	CC	33.2	2	2.169	[63]
	CS			2.572	
	CSE			2.363	
	CRH			2.264	
	CR			2.038	
	CRE			2.063	
	CE			1.995	
	CHA			1.953	
	CT			1.936	
	CP			1.818	
	CH			1.687	
	CO			3.009	
	CQC			2.701	
	CSC			2.068	
	CD			1.926	
	CF			1.722	
	CL			1.621	
CTS	2.0568				
CPS	2.1695				
Steel tube	RCFS-0-2-2	37.05	2	1.76	[57]
	RCFS-0-3-2	37.05	3	2.65	
	RCFS-0-4-2	37.05	4	2.14	
	RCFS-10-2-2	26.98	2	2.09	
	RCFS-10-3-2	26.98	3	3.13	
	RCFS-10-4-2	26.98	4	3.33	
	RCFS-20-2-2	16.72	2	3.33	
	RCFS-20-3-2	16.72	3	3.33	
	RCFS-20-4-2	16.72	4	3.33	
	RCFS-30-2-2	13.78	2	3.33	
	RCFS-30-3-2	13.78	3	3.33	
	RCFS-30-4-2	13.78	4	3.33	
Steel tube	C40-t3	40	3	1.74	[56]
	C40-t3.75	40	3.75	2.08	
	C40-t4.5	40	4.5	2.67	
	C50-t3	50	3	1.61	
	C50-t3.75	50	3.75	1.83	
	C50-t4.5	50	4.5	2.34	
	C60-t3	60	3	1.75	
	C60-t3.75	60	3.75	1.70	
	C60-t4.5	60	4.5	2.19	

Table 17: Effect of UHPC-SIP formwork on the ductility of composite column [49]

Type of SIP formwork	specimen	Core concrete strength, MPa	Thickness of plastic tube, (mm)	Ductility index
UHPC	T20L0	32.4	20	7.35
	T20S1		20	8.59
	T20C1		20	7.89
	T40L0		40	3.53
	T40S1		40	4.36
	T40S2		40	4.83

The dissipated energy of concrete-filled 3-D printed plastic SIP was calculated, representing the area under the load–strain curve for eight strain intervals as presented in Figure 12. It was found that the strains up to 0.5% represented much more than the pure elastic behavior of the specimens. Also, the ultimate loading force circular column was characterized by the highest dissipated energy equal to 48.6 J, as presented in Figure 13 [62].

Calculated dissipated energy while achieving a particular strain of a column is presented in Figure 13. Strains up to 0.5% represent much more than the pure elastic behavior of the specimens. For the ultimate loading force circular column with a cross-section is characterized by the highest dissipated energy equal to 48.6 J.

From Figure 14, it can be noticed that the improvement of the concrete strength is associated with a reduction in the ductility indices of the (CFAT) columns [61]. Besides, the CFAT columns' ductility indices increased with the aluminum-proof stresses, as offered in Figure 15.

It was found that the presence of an aluminum alloy outer tube with excellent ductility caused continuous strain rise while the load slowly dropped after achieving the ultimate strengths, and the load-strain curve of the concrete-filled aluminum tube (CFAT) was roughly horizontal [60].

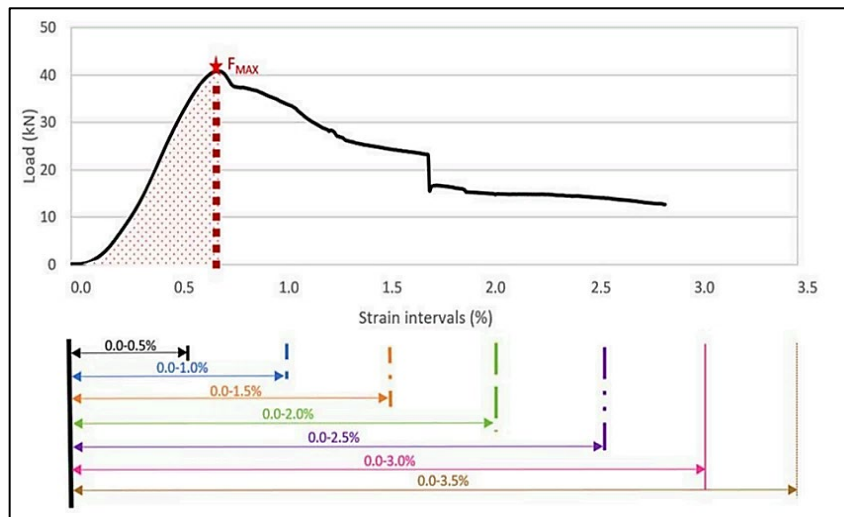


Figure 12: Position of strains for measuring dissipated energy [62]

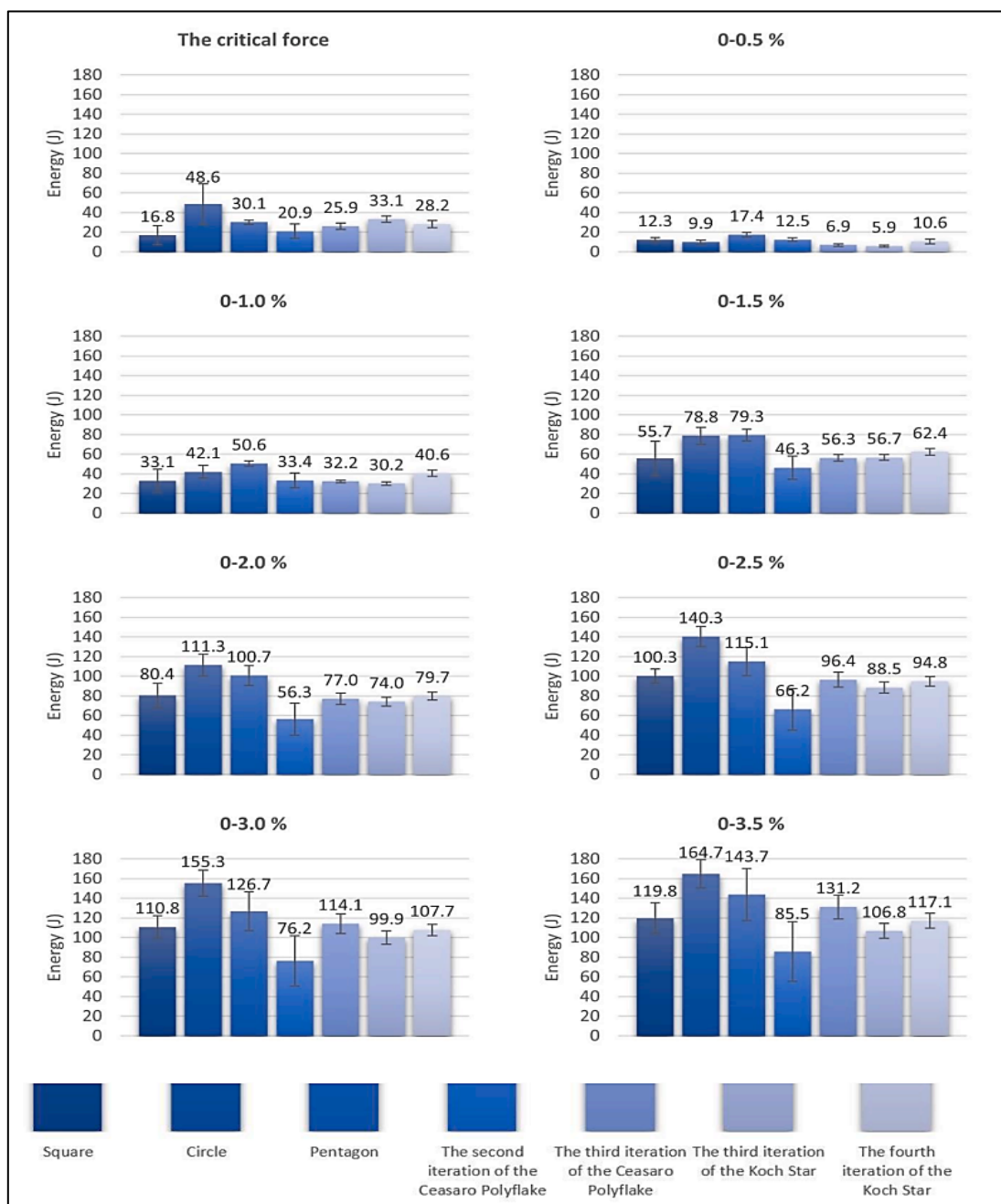


Figure 13: Dissipated energy while achieving particular column strain [62]

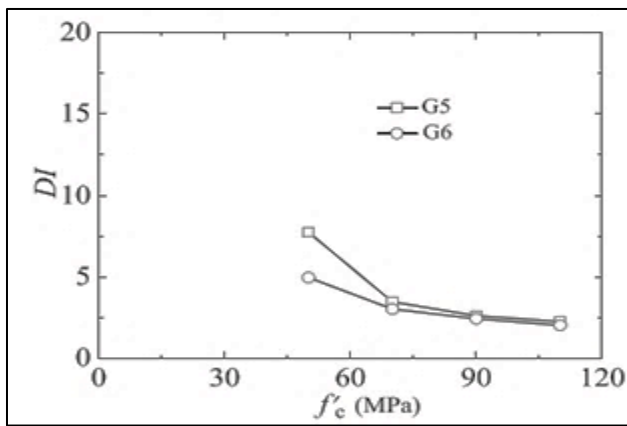


Figure 14: Effects of concrete strength on the ductility indices of CFAT short columns [61]©2022Elsevier

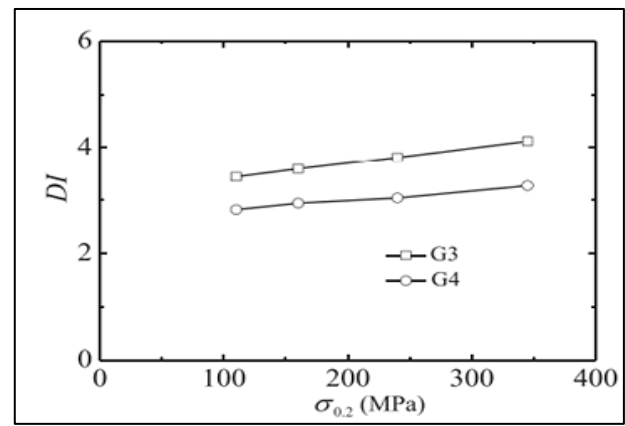


Figure 15: Effects of aluminum-proof stress on the ductility indices of CFAT short columns [61]©2022 Elsevier

There was a significant improvement in the ductility and toughness of the composite columns with the SS grids, as shown in Table 17. Moreover, the softly lower ductility and toughness of T20C1 than that of T20S1 was because of the more minor ultimate tensile strain of the CFRP grid than the SS grid [49].

3D concrete printing SIP formwork for concrete column construction was studied by Zhu et al., [55]. It was clear that the compressive strength and stiffness of concrete-filled 3D printer concrete formwork columns were improved compared to the cast-in-place columns with the same reinforcement ratios. This behavior could be due to the higher compressive strength of permanent 3D printer formwork (40 MPa) than that of cast-in-place core concrete (30 MPa).

He et al. [53] demonstrated the restriction influence of various strength classes of concrete-filled steel tube columns. They found that the post-peak conduct was neatly associated with the restriction factor ($\lambda = A_s f_s / A_c f_c$) value. Thus, a larger λ paradigm offered higher ductility, illustrating the hardening or softening conduct in the axial load-deformation curves, as shown in Figure 1.

6. Conclusion

The stay-in-place (SIP) formwork, a prefabricated permanent constructional part that holds fresh concrete to the required sizes and remains in the site to support loads during the construction lifetime, may be a wise substitute for the conventional formwork process. This study reviews some types of SIP-formworks that encased reinforcement concrete columns. The following conclusions could be dragged from this investigation:

- 1) The strength of the concrete-filled permanent tube column was improved compared to the unconfined concrete column for almost all types of SIP formwork. However, with the rising of core concrete strength, there was a reduction in the confinement influence.
- 2) From the former literature review, it was obvious that UPVC tubes could be utilized as a SIP formwork column spatially in marine constructions due to the superior chemical resistance of UPVC pipes and their high impermeability.
- 3) The increase in thickness of almost all types of SIP formwork caused an increase in the load-carrying capacity and ductility index of composite columns. Moreover, the most effective thickness for steel-SIP formwork was 4.5 mm, while the most effective one for UPVC-SIP formwork was 3mm.
- 4) The increase in the thickness of SIP formwork encased normal strength core concrete caused an increase in the ultimate strength and the confinement ratio of almost all types of SIP formworks. On the other hand, the high-strength concrete core paradigms were unaffected. Moreover, the more brittle the composite columns were, the higher the UHPC-SIP formwork thickness.
- 5) The maximum compression load of the composite column was achieved with a circular cross-section for almost all types of SIP formwork.
- 6) The increase in strength core grade led to a noticeable increase in the ultimate compression strength of the composite columns of all types of SIP formwork. Moreover, the restriction effectiveness descended with the rise of the restriction core concrete strength.
- 7) Reinforcing the SIP formwork made of cementitious base materials with (CFRP) or any reinforcement grids to raise the ductility and toughness of composite columns offered a higher adequate side restrain than unreinforced ones. Also, a positive impact on brittleness lowering was provided by supplying a higher number of layers of grids.
- 8) The Utilizing SIP formwork made of Cementous-based material or some types of concrete offered fire-proofing and higher resistance to corrosion as compared to the counterparts made of timber, steel, and plastic SIP formwork.
- 9) Using SIP formwork created from high-strength concrete (HSC) could lead to a thinner formwork that produced faster and cheaper transportation and construction. Moreover, the HSC-SIP formwork composite columns have a lesser cross-section than the standard RC columns.
- 10) The outstanding durability of SIP formwork concrete lowered the maintenance cost to resist weathering impacts. Also, UHPC-SIP formwork produced a superior bond strength between the formwork and the core concrete, which

led to no need for additional requirements for shear transfer between the formwork and the core concrete of composite columns.

- 11) Finally, the superior quality of the superior strength concrete types SIP formworks could be ensured by manufacturing the formwork in special factories to ensure superior quality and then bringing it to the construction fields for application. In this way, the whole cost of the new composite columns could be lower than the standard RC columns, saving formwork substances and time of construction and labor.

7. Recommendation for Future Studies

- 1) Most research on the stay-in-place formwork concrete column, was limited to stumpy, small-diameter paradigms measured under uniaxial compression. Outlook surveys should be developed to involve the comprehensive test of the composite columns under ideal environmental situations. For example, the effect of creep, fatigue, temperatures, and freeze/thaw cycles on the properties of concrete-filled permanent formwork columns should be tested.
- 2) There are non-special specifications for the design of concrete-filled permanent formwork. Therefore, there will be a need for more practical work, lab, and field experiments, and exhaustive knowledge from analytical and empirical surveys to promote convenient designing guidelines that will encourage the entrance of the composite modes in practice and civil concrete building works.
- 3) To better describe the structural conduct, the eccentric, lateral, and flexural loading for long and short models should be investigated in unprecedented research.
- 4) New research should cover the properties of concrete-filled stay-in-place formwork for other specimens rather than columns, such as beams, slabs, walls, and any smaller structural models.
- 5) There was very little research on the concrete type of stay-in-place formwork compared to other types like steel or polymer. Therefore, comprehensive research on the type of permanent concrete formwork should include different formwork thicknesses, other grades of concrete strength, and different types of concrete not investigated in previous research.
- 6) The research on the bond strength between permanent formwork and core cast-in-place concrete is very limited, so there should be new studies on the bond behavior and methods to increase bond strength for keeping the composite action for the concrete-filled stay-in-place formwork members.

Acknowledgment

The research program was executed without any external funding.

Author contributions

Conceptualization, Z. Abbas. I. Gorgis. and M. Hassan; methodology, I. Gorgis; software, Z. Abbas; validation, Z. Abbas. M. Hassan. and I. Gorgis; formal analysis, Z. Abbas; investigation, M. Hassan; resources, I. Gorgis; data curation, Z. Abbas; writing—original draft preparation, Z. Abbas; writing—review and editing, M. Hassan; visualization, Iq. Gorgis; supervision, M. Hassan; project administration, I. Gorgis. All authors have read and agreed to the published version of the manuscript.

Funding

No funding was received to assist with the preparation of this manuscript. (No fund organization but I will pay the fees for publishing).

Data availability statement

The data that support the findings of this study are available on request from the corresponding author.

Conflicts of interest

The authors declare that there is no conflict of interest.

References:

- [1] W. Li, X. Lin, Ding W. Bao, and Yi. M. Xie, A review of formwork systems for modern concrete construction, *Struct.*, 38 (2022) 52–63. <https://doi.org/10.1016/j.istruc.2022.01.089>
- [2] K. Devi and T. Yadav, Cost Comparison of Different Types of Formworks, *J. Build. Mater. Sci.*, 5 (2023) 32–38. <https://doi.org/10.30564/jbms.v5i1.5515>
- [3] R. Goyal, A. Mukherjee, and S. Goyal, An investigation on the bond between FRP stay-in-place formwork and concrete, *Constr. Build. Mater.*, 113 (2016) 741–751. <https://doi.org/10.1016/j.conbuildmat.2016.03.124>
- [4] Yu, L. Bai., Shi, J. Mei, Chun W. Chan, and Qian Q. Li, Compressive behavior of large-size square PEN FRP-concrete-steel hybrid multi-tube concrete columns, *Eng. Struct.*, 246 (2021) 113017. <https://doi.org/10.1016/j.engstruct.2021.113017>
- [5] Kuang Yu, Morozov E. V., Ashraf M. A., and Krishna Sh., Buckling behaviour of reinforced thermoplastic pipes under combined external pressure and bending, in *Proc 8th Australasian Congress on Applied Mechanics (ACAM 8)*, 2014.
- [6] Jun-Yun Wang and Q.-B. Yang, Investigation on compressive behaviors of thermoplastic pipe confined concrete, *Constr. Build. Mater.*, 35 (2012) 578–585. <https://doi.org/10.1016/j.conbuildmat.2012.04.017>

- [7] S. Folkman, Validation of the long life of PVC pipes, in Proceedings of the 17th International Conference on Plastics Pipes, Chicago, USA, 2014.
- [8] L.-H. Han, C.-Y. Xu, and Z. Tao, Performance of concrete filled stainless steel tubular (CFSST) columns and joints: Summary of recent research, *J. Constr. Steel Res.*, 152 (2019) 117–131. <https://doi.org/10.1016/j.jcsr.2018.02.038>
- [9] Y. Wei, C. Jiang, and Y.-F. Wu, Confinement effectiveness of circular concrete-filled steel tubular columns under axial compression, *J. Constr. Steel Res.*, 158 (2019) 15–27. <https://doi.org/10.1016/j.jcsr.2019.03.012>
- [10] F. Abed, M. AlHamaydeh, and S. Abdalla, Experimental and numerical investigations of the compressive behavior of concrete filled steel tubes (CFSTs), *J. Constr. Steel Res.*, 80 (2013) 429–439. <https://doi.org/10.1016/j.jcsr.2012.10.005>
- [11] Y. Zhang, Y. Wei, J. Bai, and Y. Zhang, Stress-strain model of an FRP-confined concrete filled steel tube under axial compression, *Thin-Walled Struct.*, 142 (2019) 149–159. <https://doi.org/10.1016/j.tws.2019.05.009>
- [12] A. Krishan, Bearing Capacity of Concrete Filled Steel Tube Columns, Sustainability of Concrete With Synthetic and Recycled Aggregates, IntechOpen, 2021. <https://doi.org/10.5772/intechopen.99650>
- [13] M. Yu, W. Liao, S. Liu, T. Wang, C. Yu, and S. Cheng, Axial compressive performance of ultra-high performance concrete-filled steel tube stub columns at different concrete age, *Struct.*, Elsevier, 55 (2023) 664–676. <https://doi.org/10.1016/j.istruc.2023.05.113>
- [14] L. Lu, T. Zhang, T. Liang, and Q. Ren, Axial compressive behavior of circular concrete-filled steel tube stub columns with steel slag coarse aggregate, *Struct.*, 51 (2023) 1893–1905. <https://doi.org/10.1016/j.istruc.2023.03.125>
- [15] Z. Liu, H. Wu, W. Ma, and Y. Lu, Steel tube filled with recycled concrete incorporating steel-fiber reinforcement and self-stressing effect, *J. Constr. Steel Res.*, 210 (2023) 108117. <https://doi.org/10.1016/j.jcsr.2023.108117>
- [16] H. Tang, L. Hou, Z. Yuan, Y. Jia, and Y. Wang, Eccentric compressive behavior of square concrete-filled stainless steel tube (CFSST) stub columns, *Struct.*, 55 (2023) 1920–1935. <https://doi.org/10.1016/j.istruc.2023.06.114>
- [17] K. Miao, Y. Wei, S. Zhang, K. Zheng, and M. Ding, Eccentric compression behavior of concrete-filled steel tube columns strengthened by CFRP/steel strip, *Eng. Struct.*, 287 (2023) 116191. <https://doi.org/10.1016/j.engstruct.2023.116191>
- [18] P. Feng, Z. Li, Y. Zou, and J.-Q. Yang, Axial compressive performance of concrete-filled steel tube stub columns with high-strength spiral confined concrete core, *Thin-Walled Struct.*, 185 (2023) 110534. <https://doi.org/10.1016/j.tws.2023.110534>
- [19] S. Wu, W. Liu, J. Zhang, W. He, and Y. Guo, Experimental and analytical investigation of square-shaped concrete-filled steel tube columns, *J. Constr. Steel Res.*, 201 (2023) 107737. <https://doi.org/10.1016/j.jcsr.2022.107737>
- [20] S. Lin, Z. Li, and Y.-G. Zhao, Behavior of eccentrically loaded circular concrete-filled steel tube stub columns with localized corrosion, *Eng. Struct.*, 288 (2023) 116227. <https://doi.org/10.1016/j.engstruct.2023.116227>
- [21] L. Guo, J. Li, C. Jia, and M. Elchalakani, Axial compression behavior of slender concrete-filled steel tubes with machining defects representing local corrosion, *Eng. Struct.*, 286 (2023) 116091. <https://doi.org/10.1016/j.engstruct.2023.116091>
- [22] T. Ozbakkaloglu and M. Saatcioglu, Seismic performance of square high-strength concrete columns in FRP stay-in-place formwork, *J. Struct. Eng.*, 133 (2007) 44–56. [https://doi.org/10.1061/\(ASCE\)0733-9445\(2007\)133:1\(44\)](https://doi.org/10.1061/(ASCE)0733-9445(2007)133:1(44))
- [23] Y.-F. Wu and Y. Wei, General stress-strain model for steel-and FRP-confined concrete, *J. Compos. Constr.* 19 (2015) 04014069. [https://doi.org/10.1061/\(ASCE\)CC.1943-5614.0000511](https://doi.org/10.1061/(ASCE)CC.1943-5614.0000511)
- [24] J. S. Onge and A. Fam, Combined torsion and axial compression loading of concrete-filled FRP tubes, *Thin-Walled Struct.* 188 (2023) 110873. <https://doi.org/10.1016/j.tws.2023.110873>
- [25] Y. Zhan, Y. Sun, W. Huang, K. Deng, and J. Sun, Interfacial behavior of segmental concrete-filled Basalt FRP tube under compression, *Constr. Build. Mater.*, 299 (2021) 123979. <https://doi.org/10.1016/j.conbuildmat.2021.123979>
- [26] G. Wang, Y. Wei, K. Miao, K. Zheng, and F. Dong, Axial compressive behavior of seawater sea-sand coral aggregate concrete-filled circular FRP-steel composite tube columns, *Constr. Build. Mater.*, 315 (2022) 125737. <https://doi.org/10.1016/j.conbuildmat.2021.125737>
- [27] Q. Hu, Y. Mei, C. Liu, S. Zhang, and Y. Wang, Confinement mechanism and compressive stress-strain behaviours of FRP-interlayer-steel confined concrete tubes, *J. Constr. Steel Res.*, 205 (2023) 107909. <https://doi.org/10.1016/j.jcsr.2023.107909>
- [28] G. Lin and S. S. Zhang, Contribution of longitudinal GFRP bars in concrete filled FRP tubular (CFFT) cylinders under monotonic or cyclic axial compression, *Eng. Struct.*, 281 (2023) 115766. <https://doi.org/10.1016/j.engstruct.2023.115766>
- [29] S. Kanwal, Q. S. Khan, M. N. Sheikh, A. U. Qazi, and M. N. S. Hadi, Axial compressive behaviour of GPC filled FRP Tubes: Experimental and analytical investigations, *Struct.*, 55 (2023) 650–663. <https://doi.org/10.1016/j.istruc.2023.06.034>
- [30] J.-K. Zhou, J.-J. Zeng, Q.-J. Liang, H.-S. Dai, and T.-H. Fan, Compressive behavior of PET FRP-confined concrete encased CFST columns, *J. Constr. Steel Res.*, 202 (2023) 107732. <https://doi.org/10.1016/j.jcsr.2022.107732>
- [31] K. C. Liu, C. Jiang, T. Yu, and J. G. Teng, Compressive behaviour of elliptical FRP tube-confined concrete columns, *Compos. Struct.*, 303 (2023) 116301. <https://doi.org/10.1016/j.compstruct.2022.116301>

- [32] J.-J. Zeng, Z. Xu, G.-M. Chen, and M.-X. Xiong, Compressive behavior of FRP-confined cruciform steel-reinforced normal- and high-strength concrete columns, *J. Constr. Steel Res.*, 210 (2023) 108046. <https://doi.org/10.1016/j.jcsr.2023.108046>
- [33] N. A. Abdulla, A state-of art-review of materials, methods, and applications of PVC-FRP-confined concrete, *Constr. Build. Mater.*, 363(2023) 129719. <https://doi.org/10.1016/j.conbuildmat.2022.129719>
- [34] H. Tian, Z. Zhou, Y. Wei, Y. Wang, and J. Lu, Experimental investigation on axial compressive behavior of ultra-high performance concrete (UHPC) filled glass FRP tubes, *Constr. Build. Mater.*, 225 (2019) 678–691. <https://doi.org/10.1016/j.conbuildmat.2019.07.204>
- [35] K. Miao, Y. Wei, F. Dong, K. Zheng, and J. Wang, Experimental study on concrete-filled steel tube columns with inner distributed seawater and sea sand concrete-filled fiber-reinforced polymer tubes under axial compression, *Compos. Struct.*, 320 (2023) 117181. <https://doi.org/10.1016/j.compstruct.2023.117181>
- [36] Y.-J. Hu, C. Jiang, W. Liu, Q.-Q. Yu, and Y.-L. Zhou, Degradation of the in-plane shear modulus of structural BFRP laminates due to high temperature, *Sens.*, 18 (2018) 3361. <https://doi.org/10.3390/s18103361>
- [37] A. M. Woldemariam, W. O. Oyawa, and T. Nyombi, Reliability assessment of axially loaded uPVC tube confined reinforced concrete columns, *Struct.*, 23 (2020) 529–538. <https://doi.org/10.1016/j.istruc.2019.11.009>
- [38] Q. Chang et al., Concrete filled double steel tube columns incorporating UPVC pipes under uniaxial compressive load at ambient and elevated temperature, *Case Stud. Constr. Mater.*, 16 (2022) e00907. <https://doi.org/10.1016/j.cscm.2022.e00907>
- [39] S. M. Askari, A. Khaloo, M. H. Borhani, and M. S. T. Masoule, Performance of polypropylene fiber reinforced concrete-filled UPVC tube columns under axial compression, *Constr. Build. Mater.*, 231 (2020) 117049.
- [40] N. A. Abdulla, Strength models for uPVC-confined concrete, *Constr. Build. Mater.*, 310 (2021) 125070. <https://doi.org/10.1016/j.conbuildmat.2021.125070>
- [41] A. Bandyopadhyay, K. K. Maurya, and A. K. Samanta, Investigation on UPVC confined RC columns with Recycled Aggregate Concrete using C&D waste, *Struct.*, 23 (2020) 279–288. <https://doi.org/10.1016/j.istruc.2019.09.015>
- [42] N. A. Abdulla, Axial strength of short concrete-filled plastic tubes, *Struct.*, 27 (2020) 1786–1800. <https://doi.org/10.1016/j.istruc.2020.07.061>
- [43] A. M. Woldemariam, W. O. Oyawa, and T. Nyombi, Structural performance of uPVC confined concrete equivalent cylinders under axial compression loads, *Buildings*, 9 (2019) 82. <https://doi.org/10.3390/buildings9040082>
- [44] C. G. Papanicolaou and I. C. Papantoniou, Mechanical behavior of textile reinforced concrete (TRC)/concrete composite elements, *J. Adv. Concr. Technol.*, 8 (2010) 35–47. <https://doi.org/10.3151/jact.8.35>
- [45] H.-Y. Kim et al., Load-deflection behaviour of concrete slab-type elements casted on stay-in-place TRC formwork,” *Compos. Struct.*, 244 (2020) 112310. <https://doi.org/10.1016/j.compstruct.2020.112310>
- [46] L. Wang, S. Yin, J. Zhu, and Z. Huang, Flexural performance of BFRP reinforced seawater sea-sand concrete beams with TRE SIP forms under a dry-wet environment, *Appl. Ocean Res.*, 130 (2023) 103442. <https://doi.org/10.1016/j.apor.2022.103442>
- [47] Z. Qiao, Z. Pan, W. Xue, and S. Meng, Experimental study on flexural behavior of ECC/RC composite beams with U-shaped ECC permanent formwork, *Front. Struct. Civ. Eng.*, 13 (2019) 1271–1287. <https://doi.org/10.1007/s11709-019-0556-0>
- [48] S. De Sutter, O. Remy, T. Tysmans, and J. Wastiels, Development and experimental validation of a lightweight Stay-in-Place composite formwork for concrete beams, *Constr. Build. Mater.*, 63 (2014) 33–39. <https://doi.org/10.1016/j.conbuildmat.2014.03.032>
- [49] H. Tian, Z. Zhou, Y. Zhang, and Y. Wei, Axial behavior of reinforced concrete column with ultra-high performance concrete stay-in-place formwork, *Eng. Struct.*, 210 (2020) 110403. <http://dx.doi.org/10.1016/j.engstruct.2020.110403>
- [50] B. A. Graybeal, Compressive behavior of ultra-high-performance fiber-reinforced concrete, *Mater. J.*, 104 (2007) 146-152, 2007. <http://dx.doi.org/10.14359/18577>
- [51] S.-F. Jiang, S.-L. Ma, and Z.-Q. Wu, Experimental study and theoretical analysis on slender concrete-filled CFRP–PVC tubular columns, *Constr. Build. Mater.*, 53 (2014) 475–487. <https://doi.org/10.1016/j.conbuildmat.2013.11.089>
- [52] W. O. Oyawa, N. K. Gathimba, and N. M. Geoffrey, “Innovative composite concrete filled plastic tubes in compression,” *Adv. Struct. Eng. Mech.*, (2015) 1–15.
- [53] L. He, S. Lin, and H. Jiang, Confinement effect of concrete-filled steel tube columns with infill concrete of different strength grades, *Front. Mater.*, 6 (2019) 71. <https://doi.org/10.3389/fmats.2019.00071>
- [54] K. Kildashti, B. Samali, and A. Malik, Experimental and numerical studies on the comparison between stay-in-place-and conventionally-formed reinforced concrete columns under concentric loading, *Constr. Build. Mater.*, 258 (2020) 119631. <https://doi.org/10.1016/j.conbuildmat.2020.119631>
- [55] B. Zhu, B. Nematollahi, J. Pan, Y. Zhang, Z. Zhou, and Y. Zhang, 3D concrete printing of permanent formwork for concrete column construction, *Cem. Concr. Compos.*, 121 (2021) 104039. <https://doi.org/10.1016/j.cemconcomp.2021.104039>

- [56] Z. Liu, D. Huang, H. Wu, Y. Lu, and X. Luo, Axial compressive behavior of steel fiber reinforced concrete-filled square steel tube stub columns, *J. Constr. Steel Res.*, 203 (2023) 107804. <https://doi.org/10.1016/j.jcsr.2023.107804>
- [57] M. Shen, W. Huang, J. Liu, and Z. Zhou, Axial compressive behavior of rubberized concrete-filled steel tube short columns, *Case Stud. Constr. Mater.*, 16 (2022) e00851.
- [58] W. Meng and K. H. Khayat, "Development of stay-in-place formwork using GFRP reinforced UHPC elements," in *International Interactive Symposium on Ultra-High Performance Concrete*, Iowa State University Digital Press, 2016. <http://dx.doi.org/10.21838/uhpc.2016.28>
- [59] A. K. Pour, A. Shirkhani, N. S. Hamzehkolaei, Y. Zhuge, and E. N. Farsangi, Performance evaluation of composite concrete-filled steel tube columns by steel fibers and different cross-section shapes: Experimental and numerical investigations, *J. Constr. Steel Res.*, 200 (2023) 107656. <https://doi.org/10.1016/j.jcsr.2022.107656>
- [60] B. Rong, X. Zhai, Z. Li, H. Cheng, A. Dong, and R. Zhang, Study on axial compression behavior of 7A04-T6 concrete-filled aluminum tubular columns, *J. Build. Eng.*, 76 (2023) 2023. <https://doi.org/10.1016/j.job.2023.107118>
- [61] X.-F. Yan, M. Ahmed, and M.-N. He, Behavior and design of axially loaded high-strength concrete-filled circular aluminum tubular short columns, *Struct.*, 44 (2022) 357–371. <https://doi.org/10.1016/j.istruc.2022.07.088>
- [62] J. Katzer and A. Skoratko, Using 3D printed formworks for the creation of steel fibre reinforced concrete-plastic columns, *Constr. Build. Mater.*, 337 (2022) 127586. <https://doi.org/10.1016/j.conbuildmat.2022.127586>
- [63] A. H. N. Almamoori, F. H. Naser, and M. K. Dhahir, Effect of section shape on the behaviour of thin walled steel columns filled with light weight aggregate concrete: Experimental investigation, *Case Stud. Constr. Mater.*, 13 (2020) e00356. <https://doi.org/10.1016/j.cscm.2020.e00356>
- [64] M. Haji, H. Naderpour, and A. Kheyroddin, Experimental study on influence of proposed FRP-strengthening techniques on RC circular short columns considering different types of damage index, *Compos. Struct.*, 209 (2019) 112–128. <https://doi.org/10.1016/j.compstruct.2018.10.088>
- [65] J. Yang, J. Wang, and Z. Wang, Rectangular high-strength concrete columns confined with carbon fiber-reinforced polymer (CFRP) under eccentric compression loading, *Constr. Build. Mater.*, 193 (2018) 604–622. <https://doi.org/10.1016/j.conbuildmat.2018.10.226>